SHORT TITLE

TURBULENT SUPERSONIC FLOW IN A CIRCULAR PIPE

Fully Developed Turbulent Supersonic Flow in a Circular Pipe
Mahesh C. Sharma
Department of Mechanical Engineering
Master's Thesis (M.Eng.)

SUMMARY

Combining the effect of friction and area change for a supersonic flow in circular pipe, a condition can be achieved to maintain constant Mach number. Such a flow has certain invariances in the flow direction eliminating the predominant 'history' effect. It is felt that these types of flow will promote the understanding of turbulent shear flow in supersonic cases.

Initially, a simple one-dimensional theory is applied relating the total reservoir pressure and local static pressure to Mach number and friction factor. The value of half the divergence angle for maintaining the constant Mach number of about 1.65 was found to be 17 minutes. Subsequently detailed shear flow measurements were made.

In order to check the validity of point to point mapping of compressible turbulent boundary layer flow into equivalent incompressible flow as suggested by Coles' transformation theory, a correlation of velocity profile in high speed flow is carried out. It appears that profiles in compressible flow are very well correlated to law of wall. However, some discrepancy was noticed when the profiles were correlated to velocity defect law.

Temperature measurements in the shear flow show that the assumption of constant total temperature yields only 2% error in velocity distribution. The corresponding effect on the other flow parameters is negligible.

Ecoulement en cisaillement supersonique turbulent en tube circulaire
Mahesh C. Sharma
Departement de Genie Mechanique
Thèse de Maitrise (M.Eng.)

SOMMAIRE

En combinant les effets de friction avec des variations de section, il a été possible de maintenir un écoulement supersonique à l'interieur d'un tube circulaire à un nombre de Mach constant. De tels écoulements ont certaines invariances dans le sens de l'ecoulement qui éliminent les effets de 'mémoire' de l'écoulement.

On pense que l'étude de tels écoulements peut apporter une meilleure compréhension des écoulements en cisaillement supersoniques turbulents.

Une relation entre la pression totale dans le réservoir, la pression statique locale, le nombre de Mach et le facteur de friction a été obtenue par une théorie simple, basée sur la simplification d'un écoulement uni-dimensionel. Il a été trouvé que la moitié de l'angle de divergence nécessaire afin de maintenir un nombre de Mach constant de 1.65 était de 17 minutes. Ensuite, des mesures détaillées de l'écoulement en cisaillement ont été effectuées.

De facon à verifier la validité de la correspondence point par point d'une couche limite compressible turbulente avec un écoulement incompressible équivalent tel que suggéré par la théorie de transformation de Cole, la corrélation d'un profile de vitesse pour un écoulement à haute vitesse a été faite.

Il apparait que les profiles pour un écoulement compressible concordent très bien avec la loi de la paroi. Cependant des differences ont été notées lorsque les profile sont comparés avec la loi de perte de vitesse. Les mesures de température pour un écoulement en cisaillement montrent que si l'on suppose que la température est constante, l'on obtient une erreur de 2% seulement dans la distribution de vitesse. Les effets correspondants sur les autres paramètres de l'écoulement sont négligeables.

FULLY DEVELOPED TURBULENT SUPERSONIC FLOW IN A CIRCULAR PIPE

by

Mahesh C. SHARMA

A thesis submitted to the Faculty of Graduate Studies and Research in partial fulfillment of the requirements for the degree of Master of Engineering

Department of Mechanical Engineering
McGill University
Montreal, Quebec
March 1972

ABSTRACT

Combining the effect of friction and area change for a supersonic flow in circular pipe, a condition can be achieved to maintain constant Mach number. Such a flow has certain invariances in the flow direction eliminating the predominant 'history' effect. It is felt that these types of flow will promote the understanding of turbulent shear flow in supersonic cases.

Initially, a simple one-dimensional theory is applied relating the total reservoir pressure and local static pressure to Mach number and friction factor. The value of half the divergence angle for maintaining the constant Mach number of about 1.65 was found to be 17 minutes. Subsequently detailed shear flow measurements were made.

In order to check the validity of point to point mapping of compressible turbulent boundary layer flow into equivalent incompressible flow as suggested by Coles' transformation theory, a correlation of velocity profile in high speed flow is carried out. It appears that profiles in compressible flow are very well correlated to law of wall. However, some discrepancy was noticed when the profiles were correlated to velocity defect law.

Temperature measurements in the shear flow show that the assumption of constant total temperature yields only 2% error in velocity distribution. The corresponding effect on the other flow parameters is negligible.

ACKNOWLEDGEMENTS

The author would like to thank Professor Frank J. Zwarts, Director of Research, for his helpful advice and constant encouragement which he offered during the course of this work.

The technical help extended by W. Bischoff in setting up the experimental apparatus, is greatly appreciated. The author also wishes to express his gratitude to Messrs. L. J. Vroomen and Jack Kelly for their help in building up the instrumentation. Thanks are also due to Miss P. Bush for typing the text of this thesis.

Financial support has been provided by the National Research Council of Canada, under Grant No. A-5189.

TABLE OF CONTENTS

ABSTRACT (i)

ACKNOWLEDGEMENTS (iii)

LIST OF SYMBOLS (vii)

1.0 Introduction 1

1.0.1 The problem 1

1.0.2 The approach and organization of the thesis 2

2.0 The Transformation Between Compressible and Incompressible Turbulent Boundary Layers 5

2.1 The Transformation 8

2.1.1 The corresponding systems of equations 8

2.1.2 The continuity equation 9

2.1.3 The transport terms 10

2.1.4 The momentum equation 10

2.1.5 The law of corresponding stations 13

2.2 The Stream Function Transformation, $\sigma(x)$ for Turbulent Flow 16

2.3 Application of Transformation to Incompressible Flow 17

2.3.1 Velocity profile for incompressible flow 17

2.3.2 Reduction of experimental profile for compressible flow 17

3.0 Experimental Apparatus 20

3.0.1 Pitot measurements 22

3.0.2 Temperature measurements in shear flow 22

3.0.3 Traversing gear 23

3.1 Method of Testing 23

3.2 Calibration and Correction to Data 24

3.2.1 Calibration of pressure transducer, thermocouples and circular potentiometer (Helipot) 24

3.2.2 Static pressure hole correction 27

3.2.3 Pitot displacement effect 29

3.3 Data Acquisition 30

3.4 Data Reduction 31

3.4.1 Mach number 31

3.4.2 Friction co-efficient 32

3.4.3 Shear flow parameters 33

3.4.4 Pitot tube traverse 34

3.4.5 Integral quantities 34

3.4.6 Skin friction determination using Preston tube 35

3.4.7 Incompressible skin friction 36

4.0 Results and Discussion 38

4.0.1 Static pressure measurements 38

4.0.2 Fanno tube results 38

4.0.3	Preston tube pressure measurements and skin friction	40
4.0.4	Total temperature measurements across the flow	41
4.0.5	Shear flow measurements	42
4.0.6	Equivalent incompressible flow	43
4.0.7	Law of wall	44
4.0.8	Velocity defect law	44

4.1 Discussion of Experimental Errors 47

5.0 Conclusion 49

REFERENCES 50

TABLE I 55

TABLE II 56

FIGURES

LIST OF SYMBOLS

<u>Variables - Roman</u>

a	speed of sound
$C_f = \dfrac{\tau_w}{\frac{1}{2}\rho_\infty U_\infty^2}$	skin friction co-efficient
C_p	specific heat at constant pressure, 6006 ft. lbf/slug °R or 0.240 Btu/ lb °F
D	inside diameter of test pipe
d_p	Pitot tube diameter
d_s	static hole diameter
F	functional form, Equation 2.30
f	functional form, Equation 2.28
$\bar{f}$	friction co-efficient defined by Equation 3.10
G	mass rate of flow per unit area, lb. per sq. ft. per sec.
g	acceleration given to unit mass by unit force, ft. per sec. per sec.

h	enthalpy, ft.lb/lb.
J	No. of ft.lb in one Btu = 778.3
K	ratio of specific heat 1.4
M	Mach number
p	mean static pressure
P_p	total pressure recorded by Pitot tube
p_s	fluctuating static pressure
R	inside radius of pipe
R_g	gas constant 1716 ft.lbs/sec R°
$R_\theta = \frac{U_\infty \theta}{\nu_\infty}$	Reynolds number based on θ
R_d	Reynolds number based on pipe diameter
$R_{e\,dp}$	Reynolds number based on Pitot diameter
$R_{ds} = \left[\left(\frac{d_s}{\nu}\right)\sqrt{\frac{\tau_w}{\rho}}\right]$	Reynolds number based on static pressure hole diameter

r	variable radius of pipe
r_f	recovery factor defined by $\frac{T_{aw} - T}{T_o - T}$
T	absolute static temperature ($^\circ R$)
T_{aw}	adiabetic wall temperature ($^\circ R$)
T_t	absolute total temperature recorded by temperature probe ($^\circ R$)
U	mean velocity component in x-direction
u	fluctuating velocity component in x-direction
$U_\tau \equiv \sqrt{\frac{\tau_w}{\rho}}$	frictional velocity
v	fluctuating velocity component in r-direction
υ	specific volume cu.ft/lb.
x	co-ordinate parallel to wall in free stream direction
y	position of Pitot from wall

$\bar{y}$	reduced co-ordinates normal to flow as defined by Equation 2.33

Variables - Greek

α	half divergence angle (radians)
$\eta(x)$	radial co-ordinate transformation, defined by Equation 2.11
$\theta \simeq \frac{1}{R}\int_0^R \frac{\rho u}{\rho_\infty U_\infty}\left(1-\frac{u}{U_\infty}\right) r\,dr$	momentum thickness in compressible flow
$\bar{\theta} \simeq \frac{1}{\bar{R}}\int_0^{\bar{R}} \frac{\bar{u}}{\bar{U}_\infty}\left(1-\frac{\bar{u}}{\bar{U}_\infty}\right) \bar{r}\,d\bar{r}$	momentum thickness in incompressible flow
μ	dynamic viscosity
$\nu = \frac{\mu}{\rho}$	kinematic viscosity
$\xi(x)$	x-co-ordinate transformation, defined by Equation 2.10
ρ	density
$\sigma(x)$	stream function transformation, defined by Equation 2.9
σ_∞	defined by Equation 3.22

τ	shear stress
Ψ	stream function, defined by Equation 2.5

Subscripts

∞	conditions at center line of pipe
o	condition at reservoir
w	condition at wall

Superscripts

$-$	barred variables are the equivalent incompressible variables
$*$	evaluated at reference temperature, defined by Equation 3.1

1.0 Introduction

1.0.1 The problem

In a constant area pipe, the friction forces cause the Mach number to go to one (i.e. choking), but if the area is increased, the Mach number tends to go up in supersonic flow. Combining these two effects, a condition can be achieved to maintain constant Mach number in a suitably designed diverging section.

The importance of such a flow is that it will have a certain invariance in the flow direction eliminating the 'history' effect prominent in turbulent flows. Such equilibrium or 'self preserving' flows have proved to be invaluable in the understanding of incompressible turbulent shear flows and it is felt that similar understanding may be promoted for supersonic case.

Brevoort and Rashis (1955) achieved a Constant Mach number flow at M = 1.62 in a seamless carbon steel pipe of 7.875 inches inside diameter by introducing a Mahogany center body. The main aim for these experiments was to obtain some information about heat transfer co-efficients and temperature recovery factors for supersonic speeds, and no attempt was made to obtain flow measurements.

While studying loss mechanism in a low temperature crossfield plasma accelerator, Richmond and Goldstein (1966) obtained a constant Mach number flow at M = 1.4 in a rectangular channel of 1 cm^2 cross-section. Because the size of channel was so small, the direct measurements of the flow were not possible.

The present thesis is concerned with achieving a constant Mach number flow at $M \approx 1.65$ for about 16 diameters and subsequent more detailed measurements of the flow. The measurements include velocity profile, temperature profile and the measurement of surface shear using Preston tubes.

Since there is scarcity of data in literature for shear flow measurements in supersonic flows, especially in pipes, it is hoped that the present thesis will make a contribution, particularly in view of the interest in Compressible Channel flow involved in Magneto-Hydro dynamics generators and accelerators, supersonic diffusers, supersonic diffusion flames and in supersonic combustion chambers.

1.0.2 The approach and organization of the thesis

Initially a simple one dimensional theory was applied relating total pressure and local static pressure to Mach number and friction factor. The preliminary investigations were started with a straight brass tube honed to 0.726 inches inside diameter and 38 inches (52 dia.) long. It was gradually cut back in steps to get shock free flow.

Using the influence co-efficient tables given by Shapiro (1953), an initial design of diverging section was worked out and tried for constant Mach number flow. Two different trials were made and it was found necessary to adjust the expansion angle. The final test section consists of 19" long (26 diameter) straight brass tube and a diverging section 12" long (16 diameter) with diverging angle of 34 minutes.

Subsequently, two points were selected in constant Mach number regions and Pitot survey of velocity profile, temperature profile and turbulent shear flow measurements were made.

Since no experimental results or theoretical predictions exist for such flow for comparison, another approach is to look for a mathematical transformation which reduces the compressible equations to a corresponding incompressible form. This then enables the use of incompressible methods in solving the problem. The transformation technique used is essentially that of Coles (1962). Basic to the transformation theory is the assumption that the two flows are related to one another according to three scaling parameters $\sigma(x)$, $\eta(x)$, and $\xi(x)$. The first relates the stream functions in two flows, the second a multiplicative factor of Dorodnitsyn-Howarth density scaling and the third relates the streamwise co-ordinates in two flows. The transformation is developed for pipe flow in Chapter 2.

Nikuradse-Karman universal Law of Friction for smooth pipe is used to obtain incompressible friction co-efficient. This law has been verified by Nikuradse (1932) experimentally up to Reynolds number of 3.4×10^6. The results are presented in terms of two constant density flow laws, i.e., law of wall and velocity defect law.

2.0 The Transformation Between Compressible and Incompressible Turbulent Boundary Layers

The treatment of the turbulent boundary layer equations is a difficult problem. Even for incompressible flow, theorists have had to rely mostly on experimental data in order to make assumptions which would simplify the analysis sufficiently to permit solution to be obtained. This situation is caused by lack of information of the turbulent mechanism itself. However, a large body of experimental data on the mean motion of the incompressible turbulent boundary layer has been gathered and correlated. From these data, acceptable skin friction formulas have been developed and put together by Schlichting (1968). Thus, it can be seen that a working understanding of the incompressible turbulent boundary layer has been achieved through the empirical approach.

The study of compressible turbulent boundary layer is quite limited at present. Experimental work on the subject is scarce. Accurate work is limited to the case of flat plate, zero pressure gradient and nozzle wall boundary layers with or without heat transfer. However, the problem of correlating experimental results is considerably more difficult for the compressible turbulent boundary layer than for incompressible case.

One way of attacking the problem is the use of mathematical device which transforms the compressible boundary layer equations to their corresponding incompressible form. These resultant incompressible boundary layer equations can be solved by one of the methods for incompressible turbulent boundary layer flows.

For the case of laminar flow, such a transformation is known and attributed variously to Dorodnitsyn (1942a), Howarth (1948), Illingworth (1949) and Stewartson (1949). For adiabatic flow, these authors have shown that a co-ordinate transformation exists such that the equations of compressible laminar boundary layer, when expressed in the transformed variables, have nearly the same solution as for incompressible case. In fact, when product of density and viscosity is constant, the correspondence is exact. Although each author uses somewhat different form, the essence of the transformation is stretching of the co-ordinate normal to the surface, effectively replacing the variable density by a constant reference density. For flows subject to pressure gradient, stretching of longitudinal co-ordinates also takes place. However, the pressure gradient term takes the proper form for incompressible flow within a boundary layer only for adiabatic flow with Prandtl number = 1.

For the case of turbulent flow, Dorodnitsyn (1942b) and Van Le (1953) have shown that the same transformation applies for the momentum integral equation of turbulent boundary layer. Mager (1958) proposed a more complete form of transformation for turbulent flow, considering the partial differential equations of mean motion. This was later extended by Burggraf (1962) to provide a theoretical basis for the reference enthalpy method.

In all these transformation works, it has usually been assumed that stream functions in compressible flow and incompressible flow are the same at corresponding points and hence that stream lines in one flow are transformed into stream lines in other. This results in a difficulty in defining the incompressible fluid properties, often giving physically un-realistic results. Thus, this assumption of the stream function being invariant under the transformation should be relaxed. Such a transformation was derived by Coles (1962) from first principles by the wav of physical arguments by relaxing the condition for the invariance of the stream function, thereby obtaining a complete and quite general transformation of the turbulent boundary layer equations.

Coles only analysed the adiabatic wall and zero pressure gradient in detail, but stated in concluding paragraph that the transformation procedure was free from restriction and could be extended to cases including heat transfer and pressure gradient. Crocco (1963) extended the transformation to flows with arbitrary pressure gradient and heat exchange.

2.1 The Transformation

The main aim of this section is to find the correspondence between incompressible and compressible turbulent boundary layers in pipe flows. This will be done by finding a suitable set of transformations which reduce the compressible boundary layer equations to their equivalent incompressible form. The analysis deals essentially with the transformation suggested by Coles (1962) with modification for pipe flow in cylindrical co-ordinate system.

2.1.1 The corresponding systems of equations

Assuming the flow to be axi-symmetric and applying the usual boundary layer approximations, the compressible governing equations for the mean motion are

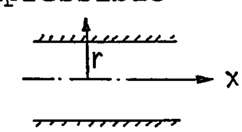

$$\rho u \frac{\partial u}{\partial x} + \rho v \frac{\partial u}{\partial r} = - \frac{dp}{dx} + \frac{1}{r}\left[\frac{\partial}{\partial r}(\tau r)\right] \tag{2.1}$$

and

$$\frac{1}{r}\frac{\partial}{\partial r}(r\rho v) + \frac{\partial(\rho u)}{\partial x} = 0 \tag{2.2}$$

The corresponding incompressible equations are

$$\bar{\rho}\bar{u} \frac{\partial \bar{u}}{\partial \bar{x}} + \bar{\rho}\bar{v} \frac{\partial \bar{u}}{\partial \bar{r}} = - \frac{d\bar{p}}{d\bar{x}} + \frac{1}{\bar{r}}\left[\frac{\partial}{\partial \bar{r}}(\bar{\tau}\bar{r})\right] \tag{2.3}$$

and

$$\frac{1}{\bar{r}}\frac{\partial(\bar{r}\bar{\rho}\bar{v})}{\partial\bar{r}} + \frac{\partial(\bar{\rho}\bar{u})}{\partial\bar{x}} = 0 \qquad (2.4)$$

where the barred quantities denote the incompressible flow variables.

2.1.2 The continuity equation

Defining the stream functions for the two corresponding flows gives

$$\left.\begin{aligned} \rho u &= \frac{1}{r}\frac{\partial\Psi}{\partial r} \qquad & \rho v &= -\frac{1}{r}\frac{\partial\Psi}{\partial x} \\ &\text{and} \\ \bar{\rho}\bar{u} &= \frac{1}{\bar{r}}\frac{\partial\bar{\Psi}}{\partial\bar{r}} \qquad & \bar{\rho}\bar{v} &= -\frac{1}{\bar{r}}\frac{\partial\bar{\Psi}}{\partial\bar{x}} \end{aligned}\right\} \qquad (2.5)$$

so that the respective continuity equations (equations 2.2 and 2.4) are automatically satisfied. The two stream functions are evidently constant on stream lines of their respective flows.*

Let the relationship between Ψ and $\bar{\Psi}$ be written as

$$\bar{\Psi}(\bar{x},\bar{r}) = \sigma(x,r)\,\Psi(x,r) \qquad (2.6)$$

where σ is a completely unspecified function of x and r.

---

* In transformation work prior to Coles', it has usually been assumed that these functions are the same at the corresponding points and hence the stream lines in one flow are transformed into stream lines in the other. This assumption often gave physicallyun-realistic results.

2.1.3 The transport terms

The formal rule for the transformation of a derivative from co-ordinates ($\bar{x}$, $\bar{r}$) to co-ordinates (x , r) may now be applied to stream function $\bar{\Psi}$ and the result expressed in terms of velocities with the aid of equation 2.5. It is found that at corresponding points in the two flows

$$\rho u = \frac{1}{\sigma}\frac{\bar{r}}{r}\left[\bar{\rho}\bar{u}\frac{\partial \bar{r}}{\partial r} - \bar{\rho}\bar{v}\frac{\partial \bar{x}}{\partial r}\right] - \frac{\Psi}{r\sigma}\frac{\partial \sigma}{\partial r} \tag{2.7}$$

and

$$\rho v = \frac{1}{\sigma}\frac{\bar{r}}{r}\left[\bar{\rho}\bar{v}\frac{\partial \bar{x}}{\partial x} - \bar{\rho}\bar{u}\frac{\partial \bar{r}}{\partial x}\right] + \frac{\Psi}{r\sigma}\frac{\partial \sigma}{\partial x} \tag{2.8}$$

2.1.4 The momentum equation

Coles (1962) showed that a correspondence between the two systems (Equation 2.1 and 2.2 vs Equation 2.3 and 2.4) can be established by defining the following transformations:

$$\frac{\bar{\Psi}}{\Psi} = \sigma(x) \tag{2.9}$$

$$\frac{d\bar{x}}{dx} = \xi(x) \tag{2.10}$$

$$\frac{\bar{\rho}}{\rho}\frac{\bar{r}}{r}\frac{\partial \bar{r}}{\partial r} = \eta(x) \qquad (2.11)$$

where σ , ξ and η are dimensionless functions of x , yet to be determined.

From equation 2.7 and 2.8, it follows that

$$\bar{u} = \left(\frac{\sigma}{\eta}\right) u \qquad \text{or} \qquad \frac{\bar{u}}{\bar{U}_\infty} = \frac{u}{U_\infty} \qquad (2.12)$$

and

$$\bar{v} = \frac{r}{\bar{r}}\frac{\rho}{\bar{\rho}}\frac{\sigma}{\xi} v + \frac{\sigma}{\xi\eta} u \frac{\partial \bar{r}}{\partial x} - \frac{\psi}{\bar{\rho}\bar{r}}\frac{1}{\xi}\frac{d\sigma}{dx} \qquad (2.13)$$

substitution of this velocity transformation (Equations 2.12 and 2.13) in the transport terms of the compressible momentum equation (2.1) yields the following:

$$\rho\left(u\frac{\partial u}{\partial x} + v\frac{\partial u}{\partial r}\right) = \bar{\rho}\left(\bar{u}\frac{\partial \bar{u}}{\partial \bar{x}} + \bar{v}\frac{\partial \bar{u}}{\partial \bar{r}}\right)\frac{\rho}{\bar{\rho}}\frac{\xi\eta^2}{\sigma^2}$$

$$+ \rho u^2 \frac{d}{dx}\left(\ln\frac{\eta}{\sigma}\right) + \frac{\psi}{r}\frac{\partial u}{\partial r}\frac{d\ln\sigma}{dx}$$

$$= -\frac{dp}{dx} + \frac{1}{r}\left[\frac{\partial}{\partial r}(\tau r)\right] \qquad (2.14)$$

or alternatively operating on corresponding incompressible terms

$$\bar{\rho}\left(\bar{u}\frac{\partial \bar{u}}{\partial \bar{x}} + \bar{v}\frac{\partial \bar{u}}{\partial \bar{r}}\right) = \frac{\bar{\rho}}{\rho}\frac{\sigma^2}{\xi\eta^2}\left\{-\frac{dp}{dx} + \frac{1}{r}\left[\frac{\partial}{\partial r}(\tau r)\right]\right.$$

$$\left. - \rho u^2 \frac{d}{dx}\left(\ln\frac{\eta}{\sigma}\right) - \frac{\psi}{r}\frac{\partial u}{\partial r}\frac{d\ln\sigma}{dx}\right\}$$

$$= -\frac{d\bar{p}}{d\bar{x}} + \frac{1}{\bar{r}}\left[\frac{\partial}{\partial \bar{r}}(\bar{\tau}\bar{r})\right] \qquad (2.15)$$

The right-hand side of equation 2.15 consists of two terms, $\frac{d\bar{p}}{d\bar{x}}$ and $\frac{1}{\bar{r}}\left[\frac{\partial}{\partial \bar{r}}(\bar{\tau}\bar{r})\right]$. The term $\frac{d\bar{p}}{d\bar{x}}$ is a function of only $\bar{x}$ (or x) and the shear stress term, i.e., $\frac{\partial(\bar{\tau}\bar{r})}{\partial \bar{r}}$ must vanish at the center line of pipe, i.e., $\bar{r} = 0$ (or $r=0$). It therefore, follows immediately that the transformed quantities $\bar{p}$ and $\bar{\tau}$ have to be defined by

$$\frac{d\bar{p}}{d\bar{x}} = \frac{\bar{e}\,\sigma^2}{\xi\,\eta^2}\left[\frac{1}{e_\infty}\frac{dp}{dx} + U_\infty^2\frac{d}{dx}\left(\ln\frac{\eta}{\sigma}\right)\right] \tag{2.16}$$

and

$$\frac{1}{\bar{r}}\left[\frac{\partial(\bar{\tau}\bar{r})}{\partial\bar{r}}\right] = \frac{\bar{e}\,\sigma^2}{\xi\,\eta^2}\left\{\frac{1}{e}\left[\frac{1}{r}\frac{\partial(\tau r)}{\partial r} - \frac{\psi}{r}\frac{\partial u}{\partial r}\frac{d\ln\sigma}{dx}\right]\right.$$

$$\left. + \frac{dp}{dx}\left(\frac{1}{e_\infty} - \frac{1}{e}\right) + \left(U_\infty^2 - u^2\right)\frac{d\left(\ln{}^{\eta}/_{\sigma}\right)}{dx}\right\} \tag{2.17}$$

respectively.

Since no particular restriction about the wall conditions has been made, this relation (equation 2.17) is valid equally for rough and smooth walls.

The transformation at this stage is not in a useful form as nothing is known about the properties of three sealing functions $\sigma(x)$, $\xi(x)$ and $\eta(x)$ which are to be specified for a particular case. However, the scope of the present thesis concerns the correlation of velocity profiles obtained from experiments in high speed flows with nominally constant Mach number and without heat transfer. Within this scope it is found unnecessary to specify explicitly $\xi(x)$ and $\eta(x)$.

Coles (1962) derived a very important relation which is called the Law of Corresponding Stations for the boundary layer on a smooth wall and is obviously of considerable value in any use of experimental data to test the validity of the present transformation for the case of turbulent flow. This is discussed in the following section.

2.1.5 The law of corresponding stations

So far the viscosity $\bar{\mu}$ in incompressible flow is not introduced, which plays a primary role. This is done by assuming the Newtonian friction at the wall and making use of relation

$$\bar{\tau} = \bar{\mu} \left(\frac{\partial \bar{u}}{\partial \bar{r}} \right)$$

Now consider the boundary layer on a smooth wall of a pipe where it is assumed for convenience that $r = \bar{r} = R(\bar{R})$. Whether the flow is turbulent or laminar, the condition

$$\left.\begin{aligned} \bar{\tau}_w &= \bar{\mu}_w \left(\frac{\partial \bar{u}}{\partial \bar{r}} \right)_{\bar{r}=\bar{R}} \\ \text{and} \qquad \tau_w &= \mu_w \left(\frac{\partial u}{\partial r} \right)_{r=R} \end{aligned}\right\} \qquad (2.18)$$

will hold at the wall.

By making use of equations 2.11 and 2.12, the shear stress in two flows, i.e. $\bar{\tau}_w$ and τ_w can be related as

$$\bar{\tau}_w = \frac{\bar{\rho}\bar{\mu}}{\rho_w \mu_w} \frac{\sigma}{\eta^2} \tau_w \qquad (2.19)$$

Local skin friction co-efficients defined by

$$\left.\begin{aligned} C_f &\equiv \frac{\tau_w}{\frac{1}{2}\rho_\infty U_\infty^2} \\ \text{and} \qquad \bar{C}_f &\equiv \frac{\bar{\tau}_w}{\frac{1}{2}\bar{\rho}_\infty \bar{U}_\infty^2} \end{aligned}\right\} \qquad (2.20)$$

or alternatively satisfy

$$C_f = \frac{2\tau_w}{\rho_\infty U_\infty^2} = 2\frac{\sigma \mu_w}{\bar{\mu}} \frac{\rho_w}{\rho_\infty} \frac{\bar{\tau}_w}{\bar{\rho}\, \bar{U}_\infty^2} = \frac{\sigma \mu_w}{\bar{\mu}} \frac{\rho_w}{\rho_\infty} \bar{C}_f \qquad (2.21)$$

Upon introducing the conventional momentum thicknesses in two flows, i.e., in compressible flow

$$\theta \simeq \frac{1}{R}\int_0^R \frac{\rho u}{\rho_\infty U_\infty}\left(1-\frac{u}{U_\infty}\right) r\,dr \tag{2.22}$$

and corresponding $\bar{\theta}$ in barred flow

$$\bar{\theta} \simeq \frac{1}{\bar{R}}\int_0^{\bar{R}} \frac{\bar{u}}{\bar{U}_\infty}\left(1-\frac{\bar{u}}{\bar{U}_\infty}\right) \bar{r}\,d\bar{r} \tag{2.23}$$

are then found to satisfy

$$\bar{\theta} = \frac{\rho_\infty}{\bar{\rho}}\eta\,\theta \tag{2.24}$$

The Reynolds number based on θ and $\bar{\theta}$ may be defined in the usual way and connected by the relation

$$R_\theta = \frac{\rho_\infty U_\infty}{\mu_\infty}\theta = \frac{\bar{\mu}}{\sigma\mu_\infty}\frac{\bar{\rho}\,\bar{U}_\infty\bar{\theta}}{\bar{\mu}} = \frac{\bar{\mu}}{\sigma\mu_\infty}\bar{R}_{\bar{\theta}} \tag{2.25}$$

Eliminating σ between relations 2.21 and 2.25

$$\bar{C}_f\,\bar{R}_{\bar{\theta}} = \frac{\rho_\infty\mu_\infty}{\rho_w\mu_w}C_f\,R_\theta \tag{2.26}$$

This important relation termed the "Law of Corresponding Stations" by Coles establishes the required equivalent states between observed compressible and incompressible boundary layers.

2.2 The stream function transformation, $\sigma(x)$ for turbulent flow

As mentioned earlier, out of the three scaling functions, $\sigma(x)$, $\xi(x)$ and $\eta(x)$, only $\sigma(x)$ is very important from experimental point of view. The main objective is to determine empirically the value of combination $\frac{\bar{\mu}}{\sigma \mu_w}$, which is expressed in terms of readily measured quantities by equation 2.21, i.e.

$$\frac{\bar{\mu}}{\sigma \mu_w} = \frac{\rho_w}{\rho_\infty} \frac{\bar{C}_f}{C_f} \qquad (2.27)$$

where the local skin friction co-efficients C_f and $\bar{C}_f$ are supposedly connected by the law of corresponding stations given by the equation 2.26.

In order to use equation 2.27 to determine the skin friction co-efficient in incompressible flow ($\bar{C}_f$), when M, C_f, R_θ and the fluid properties are known in compressible flow in form of experimental data, it is necessary to know the dependence of $\bar{C}_f$ on $\bar{R}_{\bar{\theta}}$ (or on $\bar{C}_f \bar{R}_{\bar{\theta}}$) in incompressible flow. This however, could be obtained from the existing skin friction laws connecting $\bar{C}_f$ and $\bar{C}_f \bar{R}_{\bar{\theta}}$. The dependence of $\bar{C}_f$ on $\bar{C}_f \bar{R}_{\bar{\theta}}$ is shown in Fig. 25.

2.3 Application of transformation to incompressible flow

2.3.1 Velocity profile for incompressible flow

The velocity field for an incompressible flow is usually considered to be representable in terms of two similarity laws, i.e. the law of wall and the velocity defect law. The law of wall is expressed as

$$\frac{\bar{u}}{\bar{U}_{\bar{\tau}}} = f\left(\frac{\bar{Y}\,\bar{U}_{\bar{\tau}}}{\bar{\nu}}\right) \tag{2.28}$$

where $\bar{Y}$ is given by equation 2.33 and $\bar{U}_{\bar{\tau}}$ is the shearing velocity given by the expression

$$\bar{U}_{\bar{\tau}} \equiv \sqrt{\frac{\bar{\tau}_w}{\bar{\rho}}} \tag{2.29}$$

The velocity defect law is expressed as

$$\frac{\bar{U}_\infty - \bar{u}}{\bar{U}_{\bar{\tau}}} = F\left(\frac{\bar{Y}}{\bar{R}}\right) \tag{2.30}$$

2.3.2 Reduction of experimental profile for compressible flow

Consider now that there is available a velocity profile in compressible flow at station 1 ($X = X_1$) in form of $\bar{u} = \bar{u}(\bar{x}_1, \bar{r})$. Within the forementioned assumptions, there will be flow parameters $\frac{T_w}{T_\infty}$, M_∞ and K associated with this profile. Equations 2.5, 2.9 and 2.12 are now applied to obtain $\bar{u} = \bar{u}(\bar{x}_1, \bar{r})$ and then to relate this constant density profile to law of wall and the velocity defect law given by equations 2.28 and 2.30.

Law of wall is first considered because this will lead to determination of $\bar{U}_{\bar{\tau}}$, which can be used to compute the distribution of velocity defect. By application of equations 2.11, 2.12 and 2.20, and the definition of $\bar{U}_{\bar{\tau}}$ by equation 2.29, it can be readily shown that equation 2.28 implies

$$\frac{\bar{u}}{\bar{U}_\infty} = \frac{u}{U_\infty} = \left(\frac{\bar{C}_f}{2}\right)^{\frac{1}{2}} \frac{\bar{u}}{\bar{U}_{\bar{\tau}}} = \left(\frac{\bar{C}_f}{2}\right)^{\frac{1}{2}} f\left(\frac{\bar{Y}\,\bar{U}_{\bar{\tau}}}{\bar{\nu}}\right) \tag{2.31}$$

and

$$\frac{\bar{Y}\,\bar{U}_{\bar{\tau}}}{\bar{\nu}} = \left(\frac{\bar{C}_f}{2}\right)^{\frac{1}{2}} \left[\frac{\mu_\infty \sigma}{\bar{\mu}}\right] \left(\frac{U_\infty}{\nu_\infty}\right) \frac{\theta}{\bar{\theta}}\,\bar{Y} \tag{2.32}$$

where

$$\bar{Y} = \bar{R}\left\{1 - \left[\frac{\int_0^r \frac{\rho}{\rho_\infty}\,dr^2}{\int_0^R \frac{\rho}{\rho_\infty}\,dr^2}\right]^{\frac{1}{2}}\right\} \tag{2.33}$$

With the value of $\bar{C}_f$ known from the law of corresponding stations, i.e. equation 2.26 and $\frac{\bar{u}}{\bar{U}} = \frac{u}{U}$ for compressible profile, the function $f\left(\frac{\bar{Y}\,\bar{U}_{\bar{\tau}}}{\bar{\nu}}\right)$ and

$\frac{\bar{u}}{\bar{U}_{\bar{\tau}}}$ are explicitly known. The value of $\frac{\bar{Y}\,\bar{U}_{\bar{\tau}}}{\bar{\nu}}$ can now be found by the applications of equations 2.27, 2.32 and 2.33. The data can now be presented in terms of constant density laws in form of $\frac{\bar{u}}{\bar{U}_{\bar{\tau}}}$ Vs $\left(\frac{\bar{Y}\,\bar{U}_{\bar{\tau}}}{\bar{\nu}}\right)$ and $\frac{\bar{U}_{\infty} - \bar{u}}{\bar{U}_{\bar{\tau}}}$ Vs $\left(\frac{\bar{Y}}{\bar{\bar{R}}}\right)$. It is noted that only the σ scaling function arises explicitly in the consideration of profile correlation.

Thus this analysis appears to provide a procedure for correlating compressible velocity profile according to transformation theory. In Section 3.4, this procedure will be evaluated in terms of available data relative to velocity profile.

3.0 Experimental apparatus

The complete arrangement of the test apparatus is shown in figures 1 to 4. Air is supplied by 3 air compressors (.3 lb/sec @100 psi) connected to same tank. At the discharge from the compressor, is a receiver to smooth out the fluctuations in the flow. The air is then allowed to pass through the air drier unit in order to remove the moisture from the air leaving the compressor. The absolute humidity of the air was maintained below a value approximately .0001 pounds of water per pound of air. A hand operated control valve and a quick shut-off valve are connected into the system before the reservoir. A copper-constantan thermocouple, a pressure gauge and a pressure transducer (0 - 100 psia range) are also connected in the line before the honeycomb, to read total temperature and total pressure.

The air stream is introduced in the test section through a rounded entrance axi-symmetric convergent-divergent nozzle of circular cross-section. The nozzle is designed by the method suggested by Foelsch (1949), using digital computer programme developed by Valenti (1961). The co-ordinates of the nozzle are shown in figure 4.

The initial test section was a piece of straight 38" lg. brass tube of 1.250 inches O.D. and honed to 0.726 inches I.D.

This was cut back gradually to get shock free flow. The final test section consists of a 19" long straight tube and 12" long diverging section with diverging angle of 34 minutes. The diverging section has two openings for traversing the Pitot tube and two small blind holes drilled to terminate very close to inner wall for the wall temperature copper-constantan thermocouple.

The Pitot openings are fitted with plugs, which were first located positively and then machined carefully along with the diverging section to avoid any interference with the flow. Holes of 1/16 inch diameter are drilled through these plugs in order to accommodate the Pitot tube and the temperature traversing probe, and can be blocked when not in use.

The static pressure measurements from which the Mach number and the co-efficient of friction are calculated, were made through brass tube of 0.015 inches I.D. press fitted into a hole of 0.030 inches diameter, drilled into test pipe wall. To avoid a burr at the inside edges of static pressure hole, the inside of the test pipe was carefully polished with fine emery cloth. Connections between the static pressure taps, scannivalve and transducers were made with 1/16 inch I.D. plastic tubing. All the pressure measurements were made through pressure transducers connected to GEPAC 4020 data acquisition system (DATAC). All the temperature measurements were made using copper-constantan thermocouples also connected to DATAC.

The air stream leaving the test section was discharged to the atmosphere through a diffuser with diverging angle of 7°.

3.0.1 Pitot measurements

The Pitot tubes used for traverse through the test pipe are shown in figure 5. There were two other tubes of larger diameters but are discarded due to unreliable readings. For the measurement of skin friction co-efficient, these Pitot tubes were shaped differently (figure 6) in order to obtain good surface touch, but the tube diameters remained unchanged.

3.0.2 Temperature measurements in shear flow

In recent years, attempts have been made to determine the total temperature in boundary layer flow. Probes of extremely small dimensions are used in order to cut down the disturbance of the flow around the probe to a minimum. Spivack (1950) at N.A.A. developed a useful probe which is described briefly by Eber (1954). A similar probe shown in figure 7 is used in present investigations. The recovery factor of this probe is assumed to be the same as that of Spivack, i.e. 0.948 and constant within ± 1 percent between Mach numbers 1.2 and 2.8.

3.0.3 Traversing gear

The photograph of traversing gear used for Pitot measurements and temperature measurements in shear flow is shown in figure 8. The position of the probe inside the pipe is obtained through a circular potentiometer (Helipot) though a dial gauge indicator is also used for guidance.

3.1 Method of Testing

The air compressor was started and sufficient time allowed to elapse to obtain steady state condition before readings were taken. Care was taken to check the junctions between nozzle exit and straight section of test pipe and between the straight section and diverging section. If the junctions are not proper, an oblique shock will form at the junction. This shock wave will extend down and across the stream until it encounters the opposite wall and then will reflect back and forth along the length of pipe and measurement of pressure variations along the test pipe become difficult to interpret. There was a slight interference at the junction of straight section and diverging section which did not effect the average quantities much, but its presence was clearly noted during the Pitot traverse at station number 1. However, 5 inches downstream i.e. at station number 2, the effect of this interference was un-noticeable.

First the total pressure, total temperature, wall temperature and static pressure readings were taken, which were used to find the average Mach number distribution and co-efficient of friction along the test section. Scannivalve was used to read the static pressure at successive ports. The motor of scannivalve received signal from DATAC to advance the opening to the next port through a relay connected in line.

In the case of Pitot tube and temperature probe traverses,this system was modified since the flow measurements were confined to one point at one time. A push button station was installed to give signals to DATAC for recording the measurements.

3.2 Calibration and Correction to Data

3.2.1 Calibration of pressure transducers, thermocouples and circular potentiometers (Helipot)

All pressure transducers were calibrated against mercury manometer for pressure below atmosphere and Dead

Weight Tester for pressures above atmospheric. Copper constantan thermocouples were calibrated against three reference points, i.e. ice temperature, room temperature and the boiling temperature. Circular potentiometer was calibrated against the known movement read-off of the dial test indicator. The following table lists the various measurements with the associated experimental range and estimated accuracy.

Measurements	Type of Instrument and Manufacturer's Range	Experimental Range	Estimated Error
Reservoir Pressure	Statham Pressure transducer 0 - 100 psia	50 - 90 psia	1% (± 0.6 psi)
Static Pressure	Statham Pressure transducer with General Design Scanni-valve 0 - 20 psia	0 - 15 psia	.5% (or ± .02 psi)
Pitot Pressure	Statham Pressure transducer 0 - 100 psia	0 - 50 psia	1% (± 0.6 psi)
Reservoir Temperature	Copper-constantan Thermocouple	70 - 80°F	(± 1.0°R)
Total Temperature across the pipe	Copper-constantan Thermocouple	50 - 85°F	(± 1.0°R)
Wall Temperature	Copper-constantan Thermocouple	40 - 60°F	(± 1.0°R)
Probe Position	Circular Potentiometer 5 k ohms	5 k ohms	± 5 ohms (± .001 inch)

3.2.2 Static pressure hole correction

Pressure measured through a finite size static pressure hole differs slightly from the true static pressure. The flow behaviour is such that the presence of hole deflects the stream line into the hole as shown in the sketch. The curvature of streamline increases the static pressure in the hole above the true value of the pipe. There is also a eddy or system of eddies set up in the hole.

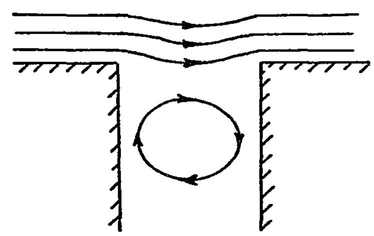

There have been many investigations of the static pressure hole error problem, mostly for incompressible flow with essentially zero pressure gradient condition. Shaw (1959) showed that the dimensionless pressure error $\left(\frac{\Delta p}{\tau_w}\right)$ is positive in turbulent flow and is function of Reynolds number $\left[\left(\frac{ds}{\nu}\right)\sqrt{\frac{\tau_w}{\rho}}\right]$ only. The dimensionless error tends to zero for small Reynolds number, but increases more rapidly with Reynolds number up to 300 and then less rapidly. For Reynolds number over 700, the quantity $\Delta p / \tau_w$ becomes almost constant at 2.75.

Rainbird (1967) investigated these errors for compressible flows and showed $\frac{\Delta p}{\tau_w} = f\left(\frac{ds}{\nu}\sqrt{\frac{\tau_w}{\rho}}\ ,\ \frac{ds}{\delta^*}\right)$

He also extended Shaw's correlation to compressible flow provided the fluid properties based on either wall or intermediate temperature are used in computation of Reynolds number $\left(\frac{d_s}{\nu}\sqrt{\frac{\tau_w}{\rho}}\right)$. This appears to remove Mach number effect, leaving relative hole size $\frac{d_s}{\delta^*}$ as parameter. Rainbird also showed that if parameter $d_s/\delta^* > 1$, it strongly influences the correlation, but for the present experiment $0.15 < \frac{d_s}{\delta^*} < 0.20$ and its influence may be safely neglected. The fluid properties are evaluated at reference temperature T^* given by

$$T^* = T_\infty \left(1 + 0.132\ M_\infty^2 \right) \tag{3.1}$$

In applying this correction, Shaw's correlation was approximated as follows:

and

$$\left.\begin{aligned} \frac{\Delta P}{\tau_w} &= 0.0045\ R_{ds} \quad \text{for} \quad 0 \leq R_{ds} \leq 611 \\ &= 2.75 \qquad\qquad \text{for } R_{ds} > 611 \end{aligned}\right\} \tag{3.2}$$

where τ_w was obtained from the Preston tube calculation in section 3.4.6 (specifically, equation 3.18). These corrections were below 1.0% in the present investigation.

3.2.3 Pitot displacement effect

When a finite size Pitot tube is placed in a pipe or boundary layer, the velocity measured does not correspond to that at the geometric center of the probe. The reason being that the Pitot pressure P_p varies non-linearly with flow velocity u (i.e. $P_p \propto u^2$). In general, it is displaced by a small distance Δy from the center in the direction of increasing flow.

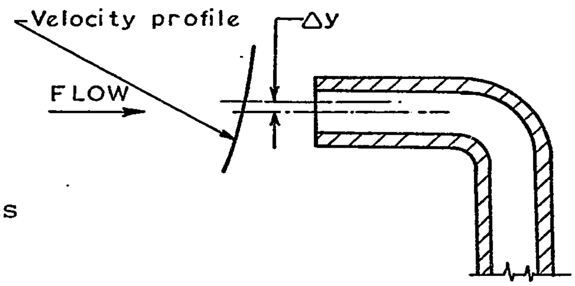

MacMillan (1956) has shown for incompressible flow that for $\frac{y}{dp} > 2$, the total correction may be expressed as displacement given by

$$\frac{\Delta y}{dp} = 0.15 \pm 0.01 \tag{3.3}$$

when $\frac{y}{dp} < 2$, an additional correction must be applied for the effect of wall. No such investigations exist for supersonic cases. However, in present data reduction following corrections were made.

$$\frac{\Delta y}{dp} = 0.15 - 0.04 \left(\frac{dp}{y} - 0.5\right) \text{for } \frac{dp}{2} \leqslant y \leqslant 2dp \tag{3.4}$$

These corrections effected the results at the most by 1.5%.

3.3 Data Acquisition

In all the investigations considered in this thesis, the McGill GEPAC 4020 Real Time Data Acquisition system (DATAC) was used for the logging of time average data. A simplified schematic diagram of the system is shown in figure 9. It is located in the instrument laboratory of the Department of Mechanical Engineering and is connected to site of present investigations by means of analog lines.

The Voltmeter and the Scanner are under program control such that mode (D.C. volts, frequency and resistance), range (10 mv - 1000 v OR 1 ohm - 10m ohm, arranged in decades) and integration time 1.6ms (50 scans/sec), 16.6 ms (25 scans/sec) and 166.6 ms (5 scans/sec) are under program control. In present investigations, D.C. volt, resistance and an integration time 166.6 ms (5 scans/sec) were used throughout. However, in few cases the readings were obtained by applying all the three integration times and it was found that the results do not vary more than 2.3%. The system was programmed to scan and record " ON DEMAND " through the use of a keyboard send and record (KSR). Four significant figures were considered in all data recording.

3.4 Data Reduction

For the application of transformation outlined in Chapter 2, the data has to be further reduced to yield:

a) Variation of Mach number and friction co-efficient with the streamwise co-ordinates.

b) Profile parameters through the shear flow as deduced from the Pitot traverse.

c) Various integral quantities such as momentum thickness (θ) and reduced co-ordinates normal to flow ($\bar{y}$)

d) Skin friction co-efficient

3.4.1 Mach number

Since the flow to the throat is isentropic and the entire flow is adiabatic, the following relation is used to calculate the Mach number:

$$\left(\frac{p}{P_o}\right)\left(\frac{A}{A^*}\right) = \frac{\frac{1}{M}\left[\left(\frac{2}{K+1}\right)\left(1+\frac{K-1}{2}M^2\right)\right]^{\frac{K+1}{2(K-1)}}}{\left(1+\frac{K-1}{2}M^2\right)^{\frac{K}{K-1}}} \qquad (3.5)$$

where A is cross-section area of pipe and A^* is area of nozzle throat.

3.4.2 Friction co-efficient

This term is intended to represent for any cross-section of the stream the quantity

$$C_f = \frac{2\,\tau_w}{\rho_\infty U_\infty^2} \tag{3.6}$$

In reality, the apparent friction co-efficient is defined in terms of measured quantities, flow per unit area and pressure through the equation

$$h_o = \frac{G^2 v^2}{2g} + \frac{K}{K+1} \times 144\, p v \tag{3.7}$$

and

(v = Specific volume, cu.ft. per lb)

$$\bar{f} = \frac{g D}{2G^2 (x_2 - x_1)} \left[\frac{C_p T_o J (K-1)}{2K} \left(\frac{1}{v_1^2} - \frac{1}{v_2^2} \right) - \frac{G^2}{g} \frac{(K+1)}{2K} \ln \frac{v_2}{v_1} \right] \tag{3.8}$$

which was derived by Keenan (1939).

In terms of L/D, K and M for a perfect gas, the equation becomes

$$\bar{f} = \frac{D}{4L} \left\{ \frac{1}{2K} \left[\frac{2 + M_1^2 (K-1)}{M_1^2} - \frac{2 + M_2^2 (K-1)}{M_2^2} \right] - \left(\frac{K+1}{K} \right) \ln \sqrt{\frac{[2 + M_1^2 (K-1)] M_2^2}{[2 + M_2^2 (K-1)] M_1^2}} \right\} \tag{3.9}$$

where

$$\bar{f} = \frac{1}{L} \int_{x=0}^{x=L} C_f \, dx \tag{3.10}$$

In the diverging section where the combined effect of friction and area change are considered

$$\tan \alpha = \frac{kM^2}{2} Cf \qquad (3.11)$$

(α = Half diverging angle in radians.)

3.4.3 Shear flow parameters

According to the boundary layer concept, the static pressure does not vary in direction normal to the flow, so that

$$T = Tt - rf\left(\frac{1}{2}\frac{u^2}{Cp}\right) \qquad (3.12)$$

where Tt is stagnation temperature in shear flow

and rf is the recovery factor of temperature measuring probe,

and

$$\rho = \frac{P}{Rg\,T} \quad \text{or} \quad \frac{\rho}{\rho_\infty} = \frac{T_\infty}{T} \qquad (3.13)$$

where Rg is gas constant for air = 1716 ft.lbf./slug/°R and

T is the temperature obtained from the temperature measuring probe by applying equation (3.12)

$$u = Ma = M\,(1{\cdot}4\,R_g T)^{1/2} \quad \text{or} \quad \frac{u}{U_\infty} = \frac{M}{M_\infty}\left(\frac{T}{T_\infty}\right)^{1/2} \qquad (3.14)$$

where M is obtained by Pitot traverse.

$$\mu = 0.381 \times 10^{-6} \left(\frac{T}{537}\right)^{3/2} \frac{735}{T + 198} \ \text{lb-sec/ft}^2 \qquad (3.15)$$

$$R_{ed} = \frac{\rho_\infty U_\infty D}{\mu_\infty} \qquad (3.16)$$

3.4.4 Pitot tube traverse

Photographs reveal that when an impact tube is placed in a supersonic stream, a curved shock wave stands ahead of mouth of the tube. The Mach number of the undisturbed stream ahead of the shock wave may be found from the following equation from measured data.

$$\frac{P_p}{P} = \left[\frac{K+1}{2} M^2\right]^{\frac{K}{K-1}} \Bigg/ \left[\frac{2K}{K+1} M^2 - 1\right]^{\frac{1}{K-1}} \qquad (3.17)$$

which reduces to

$$= 166.9216\, M^2 \Big/ \left(7 - \frac{1}{M^2}\right)^{2.5} \quad \text{for } k = 1.4$$

here the boundary layer concept of constant static pressure is assumed.

Once the local Mach number and static temperature are known, the other boundary layer parameters can be found by employing equations 3.13 to 3.15.

3.4.5 Integral quantities

The various integral quantities θ , $\bar{\theta}$ and $\bar{y}$ are determined by numerical integration(trapezoidal rule) of the traverse data. The integrand of these quantities are made up of various combinations of terms $\frac{\rho}{\rho_\infty}$, $\frac{u}{U_\infty}$ which may be readily found by the use of equations (3.13) and (3.14) respectively.

3.4.6 Skin friction determination using Preston tube

When a traversing Pitot tube of circular cross-section rests on the surface of test wall, it is termed as circular surface Pitot tube (Preston tube). Many authors have proposed correlation for Preston tubes in supersonic flow. However, the following three are used in the present data reduction.

(a) Sigalla (1965)

$$\log_{10}\left[\left(\frac{\rho^* \mu_\infty}{\rho_\infty \mu^*}\right) Re_{dp} \frac{U_p}{U_\infty}\right]^2 = 1.420 + 1.145 \log_{10}\left[\frac{\rho^*}{\rho_\infty}\left(\frac{\mu_\infty}{\mu^*}\right)^2 C_f\right] \tag{3.18}$$

where subscript $*$ refers to properties evaluated at the reference temperature T^* in equation (3.1), U_p is the velocity ahead of Preston tube obtained from equation (3.14), and Re_{dp} is the Reynolds number based on diameter of Preston tube. i.e.,

$$Re_{dp} = \frac{\rho_\infty U_\infty}{\mu_\infty} d_p \tag{3.19}$$

(b) Hopkins and Keener (1966)

$$\log_{10}\left[\left(\frac{\mu_\infty}{\mu^*}\right)^2 \frac{\rho^*}{\rho_\infty} Re_{dp}^2 \left(\frac{M_s}{M_\infty}\right)^2\right] = 1.517 + 1.132 \log_{10}\left[\left(\frac{\mu_\infty}{\mu^*}\right)^2 \frac{\rho^*}{\rho_\infty} Re_{dp}^2 C_f\right] \tag{3.20}$$

where M_s is the Mach number ahead of Preston tube obtained from equation 3.17.

(c) Fenter and Stalmach (1957)

$$\log_{10}\left[\left(\frac{\mu_\infty\,\rho_w}{\mu_w\,\rho_\infty}\right)\left(Re_{dp}/\sqrt{\sigma_\infty}\right)\sin^{-1}\left(\sqrt{\sigma_\infty}\,\frac{U_p}{U_\infty}\right)\right]^2 \tag{3.21}$$

$$= 1.568 + 1.118\,\log_{10}\left[\left(\frac{\mu_\infty}{\mu_w}\right)^2\frac{\rho_w}{\rho_\infty}\,Re_{dp}^2\,C_f\right]$$

when

$$\sigma_\infty = 1 - \frac{T_\infty}{T_{t_\infty}} \quad \text{or} \quad \frac{0.2\,M_\infty^2}{1+0.2\,M_\infty^2} \tag{3.22}$$

Of these aformentioned correlations, Sigalla's (1966) is more reliable because it incorporates the more recent data. It is, therefore, used while the remaining two are given for comparison only.

Although all these calibrations are derived from zero pressure gradient data only, Patel (1965) and Naleid (1958 and 1961) have demonstrated the validity of Preston tube calibration for incompressible and supersonic flow respectively , as long as a logarithmic region exists. Thus, it appears that the shear stress measurements obtained in adverse pressure gradient are valid. Measurements taken with the two different diameters of Pitot tubes, i.e. 0.028" and 0.016" compare closely at both the stations.

3.4.7 Incompressible skin friction

In present data reduction for computing equivalent incompressible friction co-efficient, the following relation between Cf and ReCf is used.

$$\frac{1}{\sqrt{4\bar{C}_f}} = -0.8 + 2 \log \frac{\bar{u}\,\bar{D}}{\bar{\nu}} \sqrt{4\bar{C}_f} \qquad (3.23)$$

where $\bar{u}$ denotes the mean flow velocity. This is not to be confused with the notations used elsewhere which denote incompressible flow variables.

4.0 Results and Discussion

4.0.1 Static pressure measurements

Static pressure is the basic measurement which is used for further reduction of data in terms of Mach number distribution along the pipe and shear flow measurements. Any error in its measurement will effect the results considerably. To make sure that the static pressure readings obtained through DATAC are correct, a few test runs were made using three different integration periods to obtain the static pressure. The three periods used were 5 scans per sec., 25 scans per sec. and 50 scans per sec. The final results of this verification are shown in Table I. Although the difference between these readings do not amount to more than 2.5%, the readings obtained by using the longest integration period (5 scans/sec.) were used for further reduction of data.

4.0.2 Fanno tube results

Initially the experiments were started by using a 38 inch (L/D≃52) long tube of 0.726"I.D. It was found that normal shock appears in the tube at L/D≃13, with the reservoir pressure 74.7 psia (fig. 10). Upon increasing the reservoir pressure to 84.7 psia, the position of shock moved further downstream to L/D≃22 (fig. 11). The tube was then cut to

31 inches in length ($L/D \approx 42$). It was found that at reservoir pressure 74.7 psia, the shock appeared at $L/D \approx 28$. As before, the reservoir pressure was increased to 84.7 psia and it was noted that the shock moved further downstream to $L/D \approx 33$.

The tube was again cut to 26 inches in length ($L/D \approx 36$) and the experiments were repeated as before. At reservoir pressure 74.7 psia, the shock appeared at $L/D \approx 33$, but on increasing the reservoir pressure to 84.7 psia, the flow was shock free except at the exit of the tube where an oblique shock was noted. These results are shown in fig. 10 and 11.

Finally, the tube was cut at $L/D \approx 26$ and a diverging section was attached to it. The diverging angle was 45 minutes. The Mach number distribution for this combination is shown in fig. 12. This diverging section was then replaced by another diverging section with diverging angle of 34 minutes. This combination gave fairly constant distribution of Mach number as shown in fig. 12. This latter combination was used for further shear flow measurements.

The above mentioned results indicate that an increase in value of 4 Cf L/D over its maximum value at first produces a normal shock in the pipe which gradually moves downstream as the pipe length is decreased. The increase in reservoir pressure also moves the position of shock further downstream. This is in agreement with the theory of supersonic flows in a constant area pipe with friction.

The theoretical diverging angle found by using influence co-efficient tables given by Shapiro (1953) is 29 minutes, as compared with 34 minutes obtained experimentally. The slight difference is due to change in value of friction factor Cf.

4.0.3 Preston tube pressure measurements and skin friction

Preston tubes of 4 different diameters viz. 0.060 in., 0.036 in., 0.028 in. and 0.016 were initially used for measuring the skin friction. The measurements indicated that the readings obtained from 0.060 in. and 0.036 in. dia. Preston tube were inconsistent. Hence, the readings obtained from 0.060 in. and 0.036 in. dia. were not used for further reduction of data in terms of skin friction co-efficient.

Three different correlations were used for skin friction deduction from Preston tube pressure measurements viz. Hopkins and Keener (1966), Sigalla (1965) and Fenter and Stalmach (1957).

Hopkins and Keener's correlation indicated the highest values of skin friction, whereas Fenter and Stalmach's correlation indicated the lowest values. However, the three values agree within 10%. The skin friction obtained through two different diameter Preston tubes are also in close agreement. The skin friction computed from actual static pressure measurements, is in good agreement with those obtained from Preston tube measurements.

4.0.4 Temperature measurements across the flow

The distribution of total temperature across the pipe is shown in fig. 13 and 14. The reasons of asymmetric distribution at station 1 are discussed later under Section 4.0.5. It is noted from fig. 13 that the total temperature distribution indicates a relatively large temperature gradient near the wall surface. It is also noted that total temperature in the central portion of pipe exceeds the total temperature at the center line of pipe and that of reservoir (T_o). Nothweng (1956) and Spivack (1950) obtained similar results for flat plate. Van Driest (1950) obtained similar pattern for laminar boundary layers on a flat plate at Mach number ≈ 3.0, by solving energy differential equation using Crocco's method.

In fig. 14, this distribution of total temperature ($Tt/Tt\infty$) is plotted against velocity distribution ($u/U\infty$). The variation of total temperature obtained from the following set of equations [Van Driest (1951)] is also shown for reference. It is noted that energy migrated from the region near the wall to region near the central portion of the pipe. This is in agreement with the findings of Van Driest (1951) for flat plate.

$$\frac{T}{T_\infty} = \frac{T_w}{T_\infty} - \left(\frac{T_w}{T_\infty} - 1\right)\frac{u}{U_\infty} + \frac{K-1}{2} M_\infty^2 \frac{u}{U_\infty}\left(1 - \frac{u}{U_\infty}\right) \qquad (4.1)$$

$$\frac{T}{T_\infty} = \frac{T_w}{T_\infty} - \frac{K-1}{2} M_\infty^2 \left(\frac{u}{U_\infty}\right)^2 \qquad (4.2)$$

where

$$\frac{T_t}{T_{t_\infty}} = \frac{T}{T_\infty}\left[\frac{1 + \frac{K-1}{2}M^2}{1 + \frac{K-1}{2}M_\infty^2}\right] \tag{4.3}$$

The assumption of constant total temperature across the pipe ($Tt/Tt_\infty = 1$) yields less than 2% error in velocity distribution. The corresponding error is negligible in the case of momentum thickness calculations. However, in the present data reduction the actual temperature measurements were used.

4.0.5 Shear flow measurements

The turbulent velocity and Mach number distributions across the pipe at stations 1 and 2 are shown in fig. 15 to 18 and Table II. It is noted that at station 1, the distribution is asymmetric. The boring of long taper bore of small diameters always poses problems particularly at the finishing (smaller) end, where the tool starts chattering. In present experiments, it is this end where the flow is asymmetric. However, the following investigations further conclude that the asymmetric distribution is also caused by interference at the joint of straight and diverging sections.

(a) The Mach number distribution in straight section (fig. 19) i.e., before the joint and faraway downstream, i.e., at station 2 are axisymmetric.

(b) The pipe was turned around to 180° and it is noted that there is a definite shift in Mach number distribution compared from earlier traverses. This is shown in fig. 20.

(c) The total mass flow $\int_0^R 2\pi r\,(\rho u)\,dr$ across the pipe at stations 1 and 2 is found to be in agreement within 6% for 0.028 in. dia. Pitot tube and 3.5% for 0.016 in. dia. Pitot tube.

In the absence of experimental data on fully developed turbulent supersonic flows in circular pipe, the results could not be compared. However, different runs were made to make sure that the results obtained are accurate enough before any attempt was made to transform them into equivalent incompressible flow. Accordingly, it is assumed that the data as presented, is sufficiently correct for the purpose of present investigations.

4.0.6 Equivalent incompressible flows

Once the values of $\overline{Cf}$ are obtained by applying the analysis of Chapter 2 to experimental data, the data points can be presented in terms of constant density laws, i.e. law of wall in its more usual form $\bar{u}/\bar{U}_\tau$ Vs. $\bar{y}\,\bar{U}_\tau/\bar{\nu}$ and velocity defect law $(\bar{U}_\infty - \bar{u})/\bar{U}_\tau$ Vs. $(\bar{y}/\bar{R})$.

4.0.7 Law of wall

The experimental data transformed to incompressible law of wall is shown in fig. 21 and 22. It is noted that at station 2, these are in good agreement with $\bar{u}/\bar{U}_{\bar{\tau}} = 5.75 \log (\bar{y}\,\bar{U}_{\bar{\tau}}/\bar{\nu}) + 5.0$, which supports the validity of transformation theory. The data points close to the wall are inaccurate because of error in total pressure measurement as discussed in Section 4.1. However, in general, the results may be considered satisfactory.

4.0.8 Velocity defect law

The experimental data presented in terms of law of wall in fig. 21 and 22 are shown in fig 23 and 24 in terms of velocity defect law, i.e., $(\bar{U}_\infty - \bar{u})/\bar{U}_{\bar{\tau}}$ Vs. $(\bar{y}/\bar{R})$. Also shown for comparison are the velocity defect curves that correspond to following two equations of Prandtl and Von Karman respectively.

$$\frac{\bar{U}_\infty - \bar{u}}{\bar{U}_{\bar{\tau}}} = 5.75 \log \left(\frac{\bar{R}}{\bar{y}}\right) \tag{4.4}$$

and

$$\frac{\bar{U}_\infty - \bar{u}}{\bar{U}_{\bar{\tau}}} = -\frac{1}{0.36}\left\{\ln\left[1-\sqrt{1-\frac{\bar{y}}{\bar{R}}}\right]+\sqrt{1-\frac{\bar{y}}{\bar{R}}}\right\} \tag{4.5}$$

After having satisfactory correlation of experimental data in terms of law of wall, it is surprising that there is some discrepancy when the transformation theory is applied to correlate the data to velocity defect law. It is hard to study the reasons of this discrepancy in the absence of experimental data for fully developed supersonic flows in circular pipe. However, Baronti and Libby (1966) observed similar discrepancy while correlating the available experimental data for flat plate in supersonic flows to these two incompressible similarity laws through the application of transformation theory proposed by Coles (1962). They also studied the reasons of this discrepancy in distribution of velocity defect. Some of their findings related to present investigation are discussed below.

(a) The presence of the finite size probe near the surface alters the flow as discussed in Section 4.1. Disturbances, related to experimental environment in which the profile measurements were made, might be expected to have more severe effect on the outer portion of boundary layer than on the inner portion, i.e., on the law of wall region, which is dominated by local wall condition.

(b) Some of this discrepancy with respect to the correlation of velocity defect may be attributed to insufficiently high equivalent Reynolds number, i.e., $\bar{R}_{\bar{\theta}} \equiv \left(\frac{\sigma \mu_\infty}{\bar{\mu}}\right) R_\theta < 6000$. However, in the present investigation $\bar{R}_{\bar{\theta}}$ exceeds well over 6000.

(c) Use of substructure hypothesis over the sublayer hypothesis does not remove this discrepancy since most of the data was correlated using both the hypotheses.

(d) The discrepancy may be connected with an interpretation of transformation theory itself, i.e., whether the constant density flow corresponding to compressible flow with a uniform external stream also possesses a uniform external stream.

Clearly, these conditions can be examined in detail only if more experimental data is available on fully developed supersonic pipe flow.

4.1 Discussion of experimental errors

The validity of the transformation theory depends to a great extent on the accuracy of experimental data. In the present investigations, velocity and static temperature profiles are inferred from measured total pressure and total temperature across the pipe combined with assumption of constant value of static pressure. The largest source of error resides in the difficulty of obtaining accurate total pressure measurement near the wall. The error in determining the local skin friction co-efficients at the wall is directly proportional to the error in determining the Mach number gradient at the wall. The region immediately adjacent to the wall cannot be well-defined by impact pressure measurements since the presence of the finite-size probe near the surface alters the flow, and may give incorrect readings of the true flow conditions. Thus, the faired curves of Mach number in the boundary layer subject the graphical determination of $\left(\partial M/\partial r\right)_w$ to a source of error. Matting, et al (1961) have observed in their experiment, a discrepancy which increases with the Mach number, between the measured velocity slope at the wall and more reliable skin friction measurements obtained from floating elements. They pointed out that this discrepancy to the distortion of boundary layer is due to the presence of the probe which senses higher velocity than normally expected.

The turbulent fluctuations are another source of error to Pitot measurements. The experimental measurements of these fluctuations in supersonic turbulent shear flow are scarce, non-existent for pipe flow. However, there is some early tentative work done by Morkovin (1955, 1956, 1958 and 1967), Kovasznay (1950 and 1953) and Kistler (1959) for flat plate. From these measurements, it is found that the maximum value of fluctuations is about 5 - 7%, which effects the results less than 1% in terms of velocity.

5.0 Conclusion

Constant Mach number flow could be maintained in a circular pipe by proper area expansion. Such flow is of considerable interest in connection with supersonic diffusers, supersonic combustion chambers, supersonic diffusion flames and high density magneto-fluid dynamics channel flow. One-dimensional theory for constant area pipe flow and combined effect of friction and area change is in good agreement with the experimental results.

Although the region of flow immediately adjacent to the wall cannot be well defined by impact pressure measurements, the skin friction obtained by three different correlations is in good agreement with the skin friction calculated from actual static pressure measurements.

The transformation theory suggested by Coles appears to provide a satisfactory procedure for correlating high speed velocity profile to constant density law of wall. However, some discrepancy is noted when the high speed profiles were correlated to velocity defect law. Further detailed investigations of failure to correlate velocity defect needs more experimental data and full exploitation of the transformation theory.

The assumption of constant total temperature across the pipe yields 2% error in velocity distribution which has negligible effect on other flow parameters.

References

Brevoort, M. J., and Rashis, B. (1955)
Turbulent Heat Transfer measurements at a mach number of 1.62
NACA TN 3461

Baronti, P. O., and Libby, P. A. (1966)
Velocity Profiles in Turbulent Compressible Boundary Layers
AIAA J., Vol. 4, No. 2, pp. 193-202

Burggraf, O. R. (1962)
The Compressibility Transformation and the Turbulent Boundary Layer Equations
J. Aerospace Sci., Vol. 29, No. 4, pp. 434-439

Coles, D. E. (1962)
The Turbulent Boundary Layer in a Compressible Fluid
The Rand Corporation Report R-403-PR, also in The Physics of Fluids, Vol. 7, No. 9, pp. 1403-1423

Crocco, L. (1963)
Transformation of the Compressible Turbulent Boundary Layer with Heat Exchange
AIAA J., Vol. 1, No. 12, pp. 2723-2731

Dorodnitsyn, A. (1942 a)
Laminar Boundary Layer in Compressible Fluid
Comptes Rendus (Doklady) de l'Academie des Sciences de l'U.R.S.S., Vol. 34, pp. 213-219

Dorodnitsyn, A. (1942 b)
Boundary Layer in a Compressible Gas
Prikl. Matem. Mekh., Vol. 6, pp. 449-486

Eber, G. R. (1954)
Physical Measurements in Gas Dynamics and Combustion
Article D.2 Shielded Thermocouples pp. 186-197
Princeton University Press, Princeton, N.J.

Fenter, F. W., and Stalmach, C. J. (1957)
The Measurement of Local Turbulent Skin Friction at supersonic Speeds by means of Surface Impact Pressure Probes
DRL 392, CM 878. University of Texas

Foelsch, K. (1949)
The Analytical Design of an Axially Symmetric Laval Nozzle for a parallel and Uniform Jet
J. Aeronaut. Sci. Vol. 16, No. 3, pp. 161-166

Hopkins, E. J. and Keener, E. R. (1966)
Study of Surface pitots for measuring Turbulent Skin Friction at Supersonic Mach numbers - Adiabetic Wall
NASA TN D-3478

Howarth, L. (1948)
Concerning the Effect of Compressibility on Laminar Boundary Layers and their Separation.
Proc. Roy, Soc., (London) Ser. A, Vol. 194, No. A1036

Illingworth, C. R. (1949)
Steady Flow in the Laminar Boundary Layer of a Gas
Proc. Roy. Soc., (London) Ser. A, Vol. 200, No. A1060

Keenan, J. H. (1939)
Friction Co-efficients for the Compressible Flow of Steam
Journal of Applied Mechanics, Trans. A.S.M.E., Vol. 61, pp. A11-A20

Kistler, A. L. (1959)
Fluctuation Measurements in a Supersonic Turbulent Boundary Layer
The Physics of Fluids, Vol. 2, No. 3, pp. 290-296

Kovasznay, L. S. G. (1950)
The Hot-Wire Anemometer in Supersonic Flow
J. Aeronaut. Sci.. Vol. 17, No. 9, pp. 565

Kovasznay. L. S. G. (1953)
Turbulence in Supersonic Flow
J. Aeronaut. Sci., Vol. 20, No. 10, pp. 657-674

MacMillan, F. A. (1956)
Experiments on Pitot-Tubes in Shear Flow
ARC. R and M No. 3028

Mager, A. (1958)
Transformation of the Compressible Turbulent
Boundary Layer
J. Aeronaut. Sci., Vol. 25, No. 5, pp. 305-311

Matting, F. W., Chapman, D. R., Nyholm, J. R. and Thomas, A. G.
(1961)
Turbulent Skin Friction at High Mach Numbers and
Reynolds Number in Air and Helium
NASA TR R-82

Morkovin, M. V. (1955)
Effects of High Acceleration on a Turbulent
Supersonic Shear Layer
Heat Transfer and Fluid Mechanics Institute,
Pasadena, California (Stanford University Press)

Morkovin, M. V. (1956)
Fluctuations and Hot-Wire Anemometry in Compressible
Flows
AGARDograph 24, NATO, Paris (Available from NASA)

Morkovin, M. V., and Phinney, R. E. (1958)
Extended Applications of Hot-Wire Anemometry to
High Speed Turbulent Boundary Layers
AFOSR TN-58-469, ASTIA AD-158-279, John Hopkins
University, Department of Aeronautics

Morkovin, M. V. (1962)
Effects of Compressibility on Turbulent Flows
Mechnique de la Turbulence, Colloques International
du Centre National de la Recherche Scientifique 108,
pp. 367

Naleid, J. F. (1958)
Experimental Investigation of the Impact Pressure Probe Method of Measuring Local Skin Friction at Supersonic Speeds in the presence of an Adverse Pressure Gradient
Report No. 432, CF-2739, Defense Research Laboratory, The University of Texas. Austin, Texas

Naleid, J. F. and Thompson, M. J. (1961)
Pressure-Gradient Effects on the Preston Tube in Supersonic Flow.
J. Aerospace Sci., Vol. 28, No. 12, pp. 940-944

Nikuradse, J. (1932)
GesetzmaBigkeit der turbulenten Stormung in glatten Rohren
Forseh. Arb. Ing. - Wes. No. 356

Nothwang, G. J. (1956)
An Evaluation of Four Experimental Methods for Measuring Mean Properties of a Supersonic Turbulent Boundary Layer
NACA TN No. 3721

Patel, V. C. (1965)
Calibration of the Preston Tube and Limitation on its Use in Pressure Gradients
J. Fluid Mech., Vol. 23, Part 1, pp. 185-208

Rainbird, W. J. (1967)
Errors in Measurement of Mean Static Pressure of a Moving Fluid due to Pressure Holes
Report No. DME/NAE 1967 (3) National Research Council of Canada (1967)

Richmond, J. K. and Goldstein, R. (1966)
Fully Developed Turbulent Supersonic Flow in a Rectangular Channel
AIAA J., Vol. 4, No. 8, pp. 1331 - 1336

Schliehting, H. (1968)
Boundary Layer Theory
McGraw Hill Book Co., New York

Shapiro, A. H. (1953)
The Dynamics and Thermodynamics of Compressible Fluid Flow
The Ronald Press Co., New York (Vol. I)

Shaw, R. (1959)
The Influence of Hole Dimensions on Static Pressure Measurements
J. Fluid Mech., Vol. 7, pp. 550-564

Sigalla, A. (1965)
Calibration of Preston Tubes in Supersonic Flow
AIAA J., Vol. 3, No. 8, pp. 1531

Spivack, H. M. (1950)
Experiments in the Turbulent Boundary Layer of a Supersonic Flow
North American Aviation Report AL-1052, APL/JHU CM 615

Stewartson, K. (1949)
Correlated Incompressible and Compressible Boundary Layers
Proc. Roy. Soc. (London) Series A, Vol. 200, pp. 84-100

Valenti, A. M. (1961)
A Digital Computer Programme for the Calculation of Supersonic Wind Tunnel Nozzle Co-ordinates
McGill University, MERL Memo 62-2

Van Driest, E. R. and Gollos, W. W. (1950)
On the Methods of solution of the Laminar Boundary Layer Equations.
North American Aviation Report AL-1044, APL/JHU CM-614

Van Driest, E. R. (1951)
Turbulent Boundary Layer in Compressible Fluids
J. Aeronaut. Sci., Vol. 18, No. 3, pp. 145 - 160

Van Le, N. (1953)
Transformation Between Compressible and Incompressible Boundary Layer Equations
J. Aeronaut. Sci., Vol. 20, No. 8, pp. 583 - 584.

TABLE I.... COMPARISON OF RATIO OF STATIC PRESSURE/TOTAL PRESSURE ALONG THE PIPE USING DIFFERENT INTEGRATION PERIODS.

PORT NO	5 SCANS/SEC	25 SCANS/SEC	50 SCANS/SEC	MAX DIFFERENCE (IN PERCENT)
1	0.0384	0.0381	0.0390	2.36
2	0.0400	0.0394	0.0404	2.52
3	0.0429	0.0432	0.0439	2.38
4	0.0453	0.0452	0.0447	1.34
5	0.0489	0.0484	0.0485	1.04
6	0.0516	0.0504	0.0504	2.40
7	0.0535	0.0529	0.0523	2.30
8	0.0556	0.0542	0.0543	2.55
9	0.0588	0.0578	0.0574	2.44
10	0.0610	0.0606	0.0607	0.67
11	0.0629	0.0624	0.0617	1.93
12	0.0640	0.0630	0.0626	2.20
13	0.0655	0.0645	0.0655	1.54
14	0.0674	0.0664	0.0674	1.52
15	0.0683	0.0681	0.0682	0.30
16	0.0699	0.0689	0.0687	1.76
17	0.0705	0.0705	0.0707	0.30
18	0.0700	0.0709	0.0706	1.29
19	0.0714	0.0718	0.0710	1.12
20	0.0708	0.0709	0.0713	0.70
21	0.0688	0.0695	0.0698	1.44
22	0.0663	0.0662	0.0664	0.31
23	0.0658	0.0655	0.0654	0.62
24	0.0664	0.0669	0.0666	0.75
25	0.0631	0.0635	0.0636	0.79
26	0.0620	0.0625	0.0628	1.29
27	0.0605	0.0611	0.0614	1.48
28	0.0591	0.0595	0.0598	1.18
29	0.0512	0.0516	0.0515	0.79

TABLE II...FLOW MEASUREMENTS ACROSS THE PIPE

LEGEND

PNOT	$= P_o$	reservoir pressure
TNOT	$= T_o$	reservoir temperature
TWAL	$= T_w$	wall temperature
M	$= M_\infty$	Mach number at center line of the pipe
U	$= U_\infty$	Velocity at center line of the pipe
RHO	$= \rho_\infty$	density at center line of the pipe
P	$= p$	static pressure across the pipe
T	$= T_\infty$	static temperature at center line of the pipe
COLES	$= \frac{\sigma \mu_\infty}{\bar{\mu}}$	stream function transformation
RED	$= R_d$	Reynolds number based on pipe diameter
RETH	$= R_\theta$	Reynolds number based on momentum thickness
CF	$= C_f$	skin friction co-efficient
R	$= r$	radius of pipe
U/UE	$= \frac{u}{U_\infty}$	velocity ratio
RH/RHE	$= \frac{\rho}{\rho_\infty}$	density ratio

LEGEND (CONTD.)

YB	$= \bar{y}$	reduced co-ordinates as defined by Equation 2.33
YST	$= \dfrac{\bar{y}\,\bar{U}_{\bar{\tau}}}{\bar{\nu}}$	incompressible law of the wall co-ordinates
UST	$= \dfrac{\bar{u}}{\bar{U}_{\bar{\tau}}}$	incompressible law of wall velocity
VEDEF	$= \dfrac{\bar{U}_{\infty} - \bar{u}}{\bar{U}_{\bar{\tau}}}$	incompressible velocity defect law co-ordinates

TABLE II... FLOW MEASUREMENTS ACROSS THE PIPE...

STATION- 1
PITOT NO.- 1
PITOT DIAMETER- 0.0280 INCH
I.D. OF TEST SECTION- 0.7600 INCH
PNOT= 74.63 PSIA
TNOT= 530.25 DEG R
TWAL= 508.11 DEG R

PARAMETERS AT CENTER LINE OF THE PIPE
M = 2.2099 U = 1768.3 FT/SEC RHO = 0.001370 SLUG/CU FT
P = 4.350 PSIA T = 266.5 DEG R COLES = 0.6163
RED = 692603.9 RETH = 14031.9

INTEGRAL QUANTITIES AND SKIN FRICTION FROM PRESTON TUBE
MOMENTUM THICKNESS = 0.0154 INCH
CF =0.002106 FROM SIGALLA S CORRELATION
CF =0.002175 FROM HOPKIN S AND KEENER S CORRELATION
CF =0.002018 FROM STALMACH S CORRELATION
CF =0.002100 AVERAGE = RMS DEVIATION = 0.000064
CF =0.002210 FROM STATIC PRESSURE MEASUREMENTS

EQUIVALENT INCOMPRESSIBLE VARIABLES
MOMENTUM THICKNESS = 0.0205 INCH
RETH = 8648.6
CF = 0.003100

R(IN)	M	U/UE	RH/RHE	YB	YST	UST	VEDEF
0.3800	0.0	0.0	0.5245	0.0	0.0	0.0	25.40
0.3660	1.4050	0.7520	0.8121	0.0033	63.9	19.10	6.30
0.3240	1.4088	0.7516	0.8433	0.0256	494.1	19.09	6.31
0.2890	1.4900	0.7839	0.8676	0.0420	808.6	19.91	5.49
0.2540	1.6045	0.8276	0.8930	0.0611	1176.8	21.02	4.38
0.2190	1.7885	0.8920	0.9106	0.0814	1568.6	22.66	2.74
0.1840	1.9885	0.9578	0.9384	0.1032	1989.0	24.33	1.07
0.1490	2.1591	1.0070	0.9578	0.1320	2542.2	25.58	-0.18
0.1140	2.3243	1.0426	0.9782	0.1645	3168.3	26.48	-1.08
0.0790	2.4818	1.0593	0.9968	0.2064	3976.5	26.91	-1.51
0.0450	2.1806	0.9939	1.0000	0.2572	4956.0	25.24	0.16
0.0	2.2099	1.0000	1.0000	0.3800	7320.9	25.40	0.0
0.0250	2.1978	0.9964	0.9968	0.2064	3976.5	25.31	0.09
0.0590	2.1459	0.9832	0.9782	0.1645	3168.3	24.97	0.43
0.0950	2.0854	0.9668	0.9578	0.1423	2741.4	24.56	0.84
0.1240	2.0229	0.9487	0.9384	0.1125	2166.8	24.10	1.30
0.1570	1.9461	0.9279	0.9106	0.0943	1817.0	23.57	1.83
0.1910	1.8882	0.9101	0.8930	0.0711	1369.5	23.12	2.28
0.2240	1.8141	0.8883	0.8676	0.0533	1026.9	22.56	2.84
0.2540	1.7405	0.8657	0.8433	0.0346	667.0	21.99	3.41
0.2840	1.6430	0.8341	0.8121	0.0135	259.2	21.19	4.21

TABLE II... FLOW MEASUREMENTS ACROSS THE PIPE...

STATION- 1
PITOT NO.- 2
PITOT DIAMETER- 0.0160 INCH
I.D. OF TEST SECTION- 0.7600 INCH
PNOT= 74.60 PSIA
TNOT= 531.10 DEG R
TWAL= 508.11 DEG R

PARAMETERS AT CENTER LINE OF THE PIPE
M = 2.1686 U = 1751.1 FT/SEC RHO = 0.001345 SLUG/CU FT
P = 4.350 PSIA T = 271.4 DEG R COLES = 0.6712
RED = 663387.3 RETH = 15116.3

INTEGRAL QUANTITIES AND SKIN FRICTION FROM PRESTON TUBE
MOMENTUM THICKNESS = 0.0173 INCH
CF =0.002253 FROM SIGALLA S CORRELATION
CF =0.002246 FROM HOPKIN S AND KEENER S CORRELATION
CF =0.002097 FROM STALMACH S CORRELATION
CF =0.002199 AVERAGE = RMS DEVIATION = 0.000072
CF =0.002210 FROM STATIC PRESSURE MEASUREMENTS

EQUIVALENT INCOMPRESSIBLE VARIABLES
MOMENTUM THICKNESS = 0.0230 INCH
RETH = 10145.3
CF = 0.003050

R(IN)	M	U/UE	RH/RHE	YB	YST	UST	VEDEF
0.3800	0.0	0.0	0.5342	0.0	0.0	0.0	25.61
0.3660	1.2840	0.7108	0.8027	0.0046	90.9	18.20	7.41
0.3190	1.3851	0.7498	0.8395	0.0315	628.4	19.20	6.41
0.2720	1.4597	0.7802	0.8658	0.0606	1211.1	19.98	5.63
0.2340	1.6124	0.8388	0.8927	0.0810	1618.3	21.48	4.13
0.2010	1.7823	0.8994	0.9207	0.0988	1973.4	23.03	2.57
0.1640	1.9926	0.9692	0.9452	0.1244	2485.2	24.82	0.79
0.1300	2.0911	1.0004	0.9730	0.1504	3004.1	25.62	-0.01
0.1010	2.2390	1.0325	0.9914	0.1713	3422.0	26.44	-0.83
0.0650	2.3740	1.0477	1.0010	0.2142	4277.7	26.83	-1.22
0.0300	2.1516	0.9966	1.0000	0.2627	5248.0	25.52	0.09
0.0	2.1686	1.0000	1.0000	0.3800	7590.4	25.61	0.0
0.0400	2.1669	0.9987	1.0010	0.2142	4277.7	25.58	0.03
0.0750	2.1383	0.9909	0.9914	0.1686	3367.5	25.38	0.23
0.1140	2.0840	0.9760	0.9730	0.1406	2808.9	24.99	0.62
0.1480	2.0067	0.9550	0.9452	0.1134	2266.0	24.45	1.15
0.1840	1.9326	0.9333	0.9207	0.0908	1812.9	23.90	1.71
0.2190	1.8521	0.9097	0.8927	0.0697	1392.9	23.30	2.31
0.2530	1.7700	0.8841	0.8658	0.0535	1069.3	22.64	2.97
0.2870	1.6877	0.8573	0.8395	0.0348	694.4	21.95	3.65
0.3230	1.5710	0.8177	0.8027	0.0170	338.9	20.94	4.67

TABLE II... FLOW MEASUREMENTS ACROSS THE PIPE...

STATION- 2
PITOT NO.- 1
PITOT DIAMETER- 0.0280 INCH
I.D. OF TEST SECTION- 0.8100 INCH
PNOT= 74.66 PSIA
TNOT= 531.13 DEG R
TWAL= 507.83 DEG R

PARAMETERS AT CENTER LINE OF THE PIPE
M = 2.4426 U = 1867.4 FT/SEC RHO = 0.001345 SLUG/CU FT
P = 3.900 PSIA T = 243.3 DEG R COLES = 0.6165
RED = 825021.3 RETH = 18783.7

INTEGRAL QUANTITIES AND SKIN FRICTION FROM PRESTON TUBE
MOMENTUM THICKNESS = 0.0184 INCH
CF =0.001771 FROM SIGALLA S CORRELATION
CF =0.002015 FROM HOPKIN S AND KEENER S CORRELATION
CF =0.001768 FROM STALMACH S CORRELATION
CF =0.001851 AVERAGE = RMS DEVIATION = 0.000116
CF =0.001980 FROM STATIC PRESSURE MEASUREMENTS

EQUIVALENT INCOMPRESSIBLE VARIABLES
MOMENTUM THICKNESS = 0.0249 INCH
RETH = 11581.1
CF = 0.003010

R(IN)	M	U/UE	RH/RHE	YB	YST	UST	VEDEF
0.4050	0.0	0.0	0.4791	0.0	0.0	0.0	25.78
0.3910	1.4586	0.7313	0.6952	0.0044	78.6	18.85	6.93
0.3490	1.4976	0.7458	0.7076	0.0193	346.9	19.23	6.55
0.3070	1.6058	0.7843	0.7353	0.0395	712.0	20.22	5.56
0.2670	1.7503	0.8335	0.7866	0.0593	1068.0	21.48	4.29
0.2270	1.9589	0.8950	0.8363	0.0821	1478.2	23.07	2.71
0.1880	2.1166	0.9337	0.8864	0.1046	1884.4	24.07	1.71
0.1480	2.2465	0.9612	0.9208	0.1355	2439.7	24.78	1.00
0.1080	2.3377	0.9792	0.9583	0.1703	3067.4	25.24	0.54
0.0670	2.4173	0.9945	0.9896	0.2144	3861.3	25.63	0.14
0.0270	2.4213	0.9958	1.0000	0.2724	4905.9	25.67	0.11
0.0	2.4426	1.0000	1.0000	0.4050	7293.1	25.78	0.0
0.0510	2.4148	0.9945	0.9896	0.2144	3861.3	25.63	0.14
0.0910	2.3307	0.9773	0.9583	0.1728	3112.6	25.19	0.59
0.1310	2.2199	0.9519	0.9208	0.1399	2518.7	24.54	1.24
0.1710	2.0999	0.9201	0.8864	0.1125	2026.8	23.72	2.06
0.2100	1.9478	0.8814	0.8363	0.0913	1643.9	22.72	3.06
0.2470	1.7920	0.8386	0.7866	0.0662	1191.3	21.62	4.16
0.2900	1.6194	0.7861	0.7353	0.0460	828.5	20.26	5.51
0.3210	1.5182	0.7525	0.7076	0.0285	512.9	19.40	6.38
0.3510	1.4701	0.7357	0.6952	0.0117	211.4	18.96	6.81

TABLE II... FLOW MEASUREMENTS ACROSS THE PIPE...

STATION- 2
PITOT NO.- 2
PITOT DIAMETER- 0.0160 INCH
I.D. OF TEST SECTION- 0.8100 INCH
PNOT= 74.68 PSIA
TNOT= 531.68 DEG R
TWAL= 507.83 DEG R

PARAMETERS AT CENTER LINE OF THE PIPE
M = 2.3676 U = 1840.6 FT/SEC RHO = 0.001301 SLUG/CU FT
P = 3.900 PSIA T = 251.6 DEG R COLES = 0.6935
RED = 764667.7 RETH = 18317.5

INTEGRAL QUANTITIES AND SKIN FRICTION FROM PRESTON TUBE
MOMENTUM THICKNESS = 0.0194 INCH
CF =0.001949 FROM SIGALLA S CORRELATION
CF =0.002076 FROM HOPKIN S AND KEENER S CORRELATION
CF =0.001868 FROM STALMACH S CORRELATION
CF =0.001964 AVERAGE = RMS DEVIATION = 0.000086
CF =0.001980 FROM STATIC PRESSURE MEASUREMENTS

EQUIVALENT INCOMPRESSIBLE VARIABLES
MOMENTUM THICKNESS = 0.0263 INCH
RETH = 12702.9
CF = 0.002950

R(IN)	M	U/UE	RH/RHE	YB	YST	UST	VEDEF
0.4050	0.0	0.0	0.4954	0.0	0.0	0.0	26.04
0.3910	1.3168	0.6891	0.7097	0.0045	83.5	17.94	8.10
0.3540	1.4567	0.7419	0.7282	0.0167	310.8	19.32	6.72
0.3130	1.5157	0.7649	0.7505	0.0358	665.9	19.92	6.12
0.2740	1.6484	0.8129	0.7892	0.0543	1008.4	21.17	4.87
0.2330	1.8093	0.8663	0.8440	0.0774	1437.9	22.56	3.48
0.1940	2.0253	0.9252	0.8904	0.1022	1900.2	24.09	1.95
0.1550	2.1517	0.9543	0.9272	0.1294	2403.9	24.85	1.19
0.1130	2.2692	0.9792	0.9628	0.1695	3149.3	25.50	0.54
0.0730	2.3198	0.9895	0.9871	0.2116	3933.2	25.76	0.27
0.0340	2.3451	0.9952	1.0000	0.2661	4945.1	25.91	0.12
0.0	2.3676	1.0000	1.0000	0.4050	7526.7	26.04	0.0
0.0450	2.3342	0.9931	0.9871	0.2116	3933.2	25.86	0.18
0.0850	2.2688	0.9788	0.9628	0.1695	3149.3	25.49	0.55
0.1250	2.1662	0.9545	0.9272	0.1338	2485.9	24.85	1.19
0.1650	2.0389	0.9192	0.8904	0.1042	1937.3	23.93	2.10
0.2050	1.8974	0.8811	0.8440	0.0811	1506.7	22.94	3.10
0.2440	1.7276	0.8322	0.7892	0.0577	1072.6	21.67	4.37
0.2840	1.5978	0.7909	0.7505	0.0543	1008.4	20.59	5.44
0.3140	1.5174	0.7636	0.7282	0.0408	757.6	19.88	6.16
0.3420	1.4456	0.7376	0.7097	0.0326	605.5	19.21	6.83

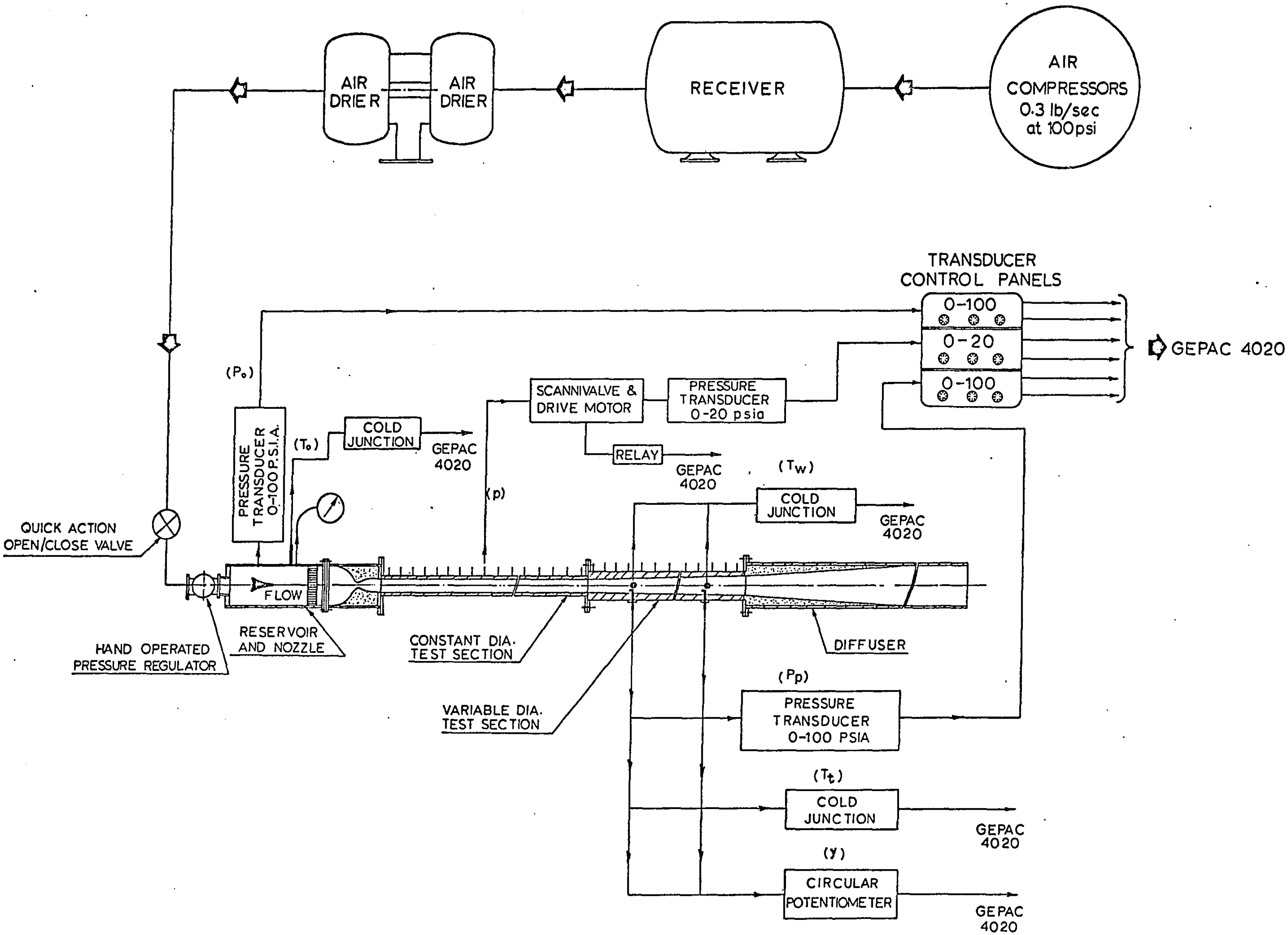

FIG. 1 — SCHEMATIC DIAGRAM OF EXPERIMENTAL SET-UP

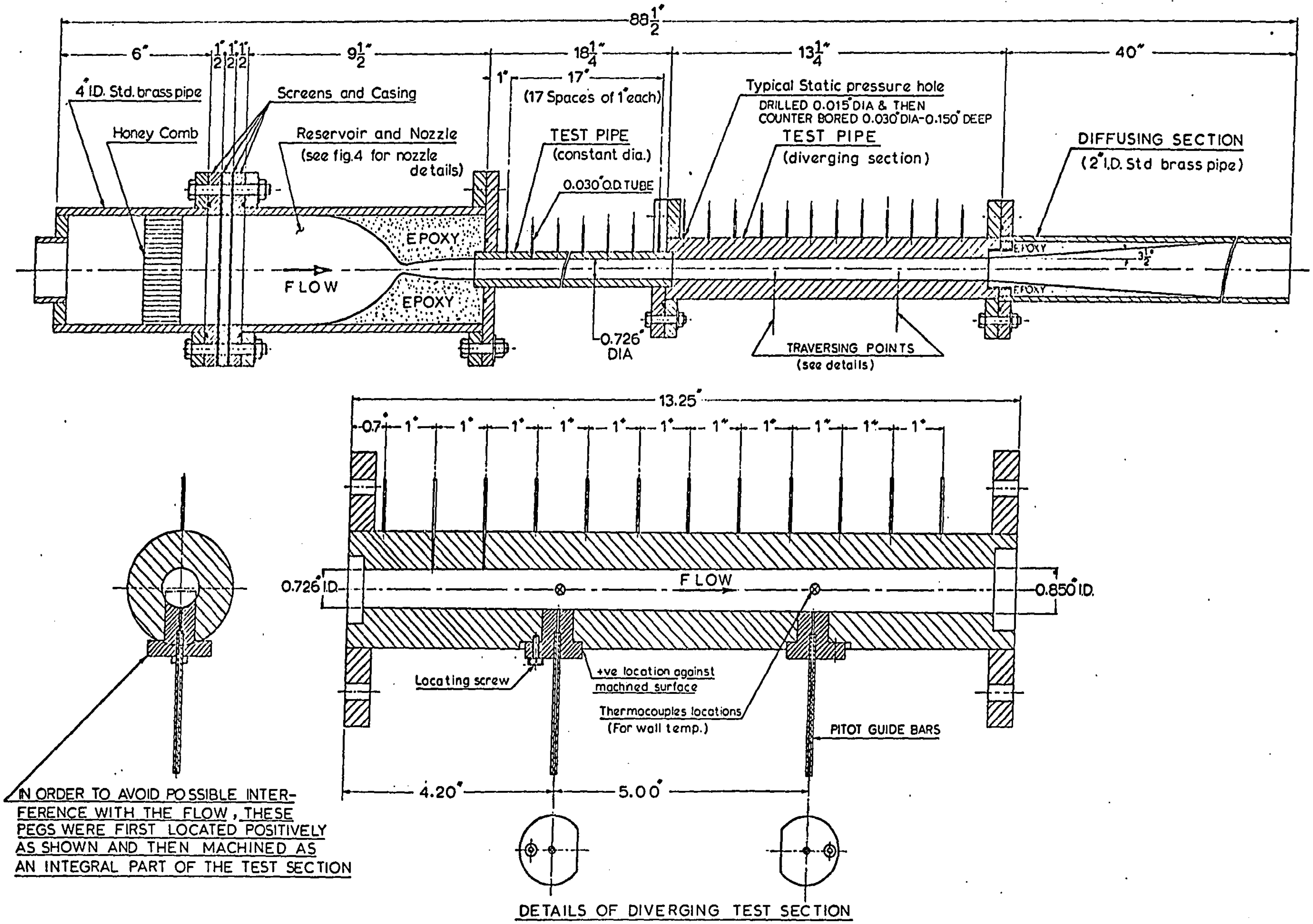

FIG.2 -GENERAL ARRANGEMENT OF THE TEST APPARATUS

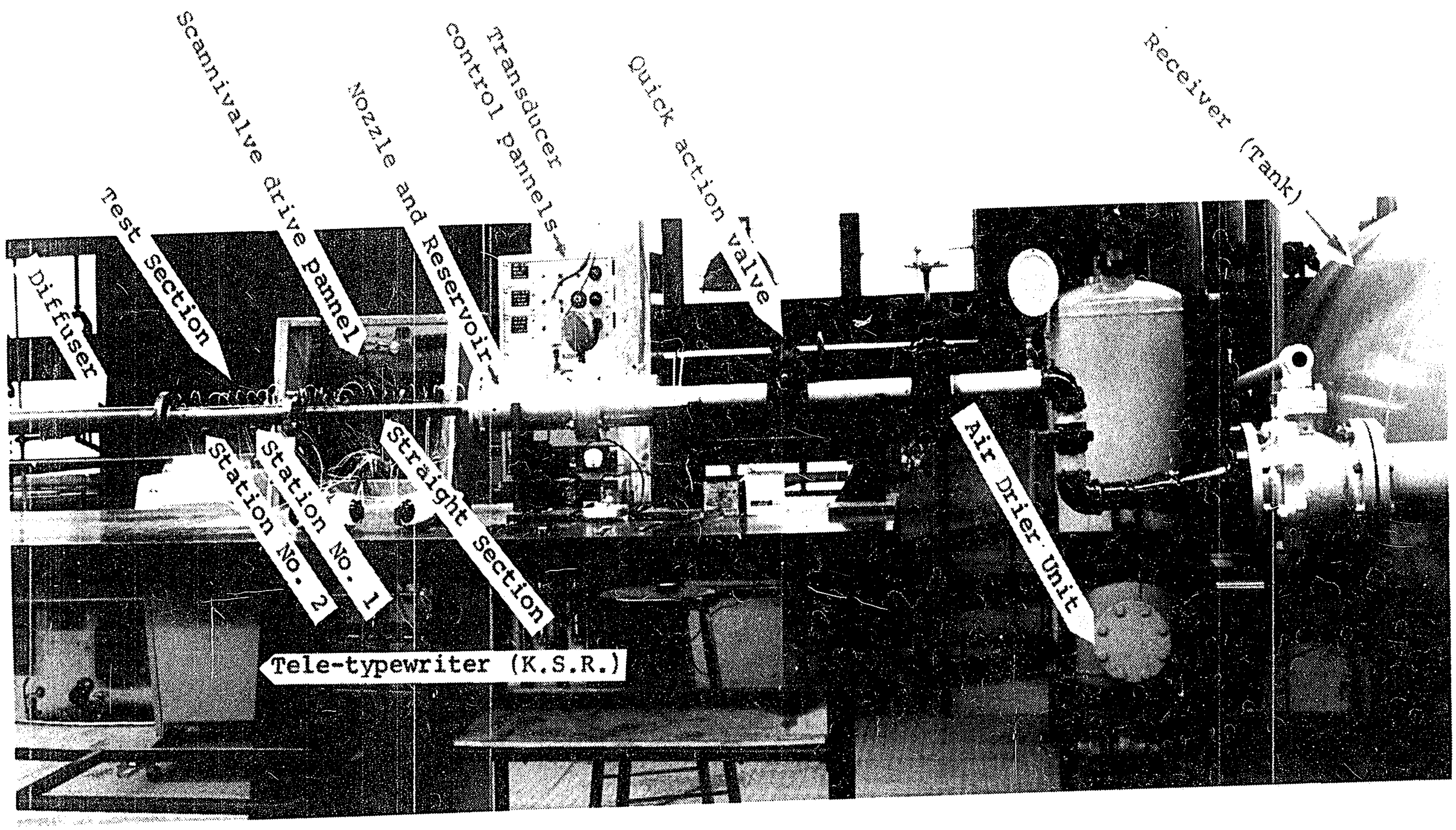

Fig. 3 - Photograph showing General Arrangement of the Experimental Apparatus.

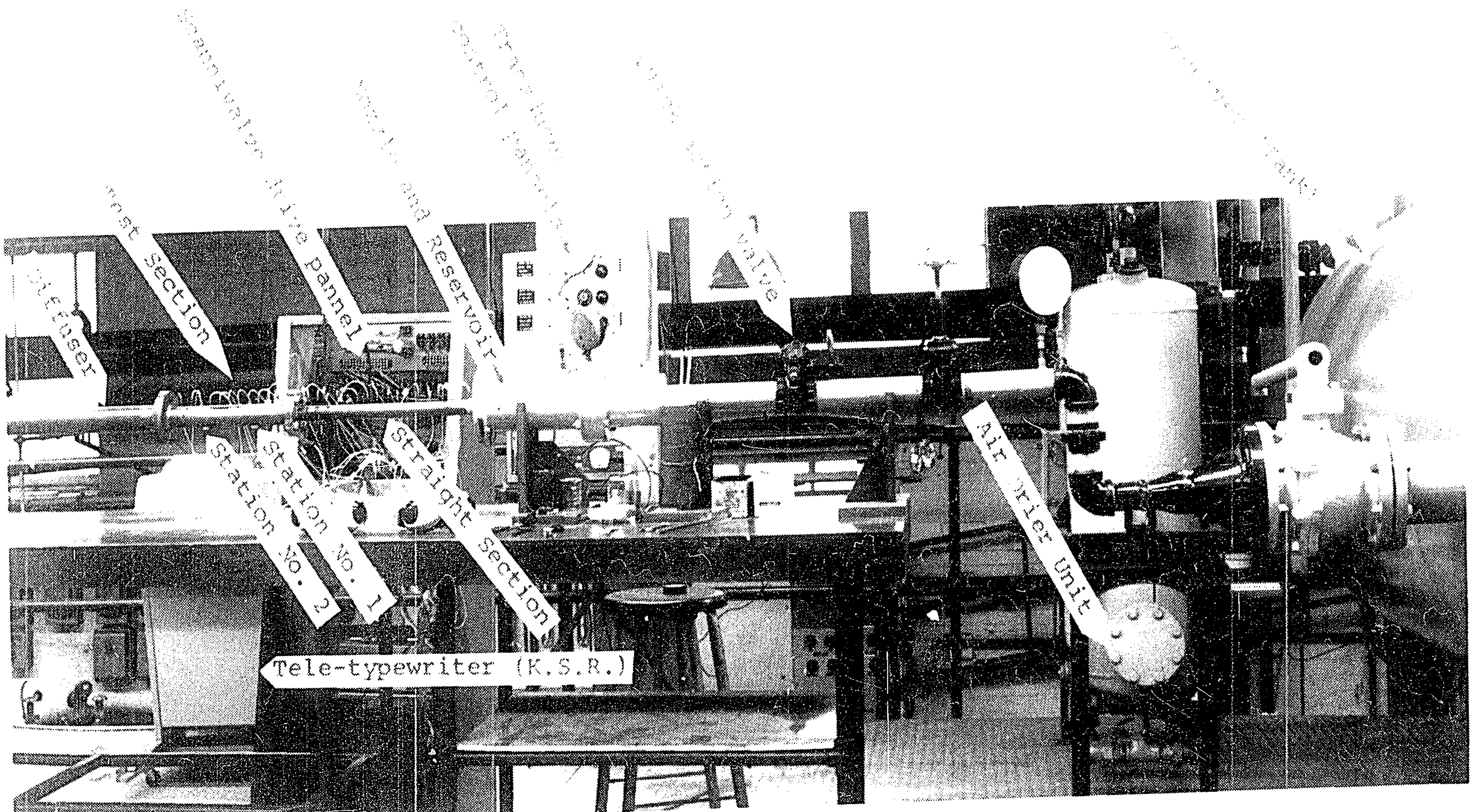
Air Drier Unit
Straight Section
Station No. 1
Station No. 2
Tele-typewriter (K.S.R.)
Test Section
Diffuser
and Reservoir
drive pannel
valve

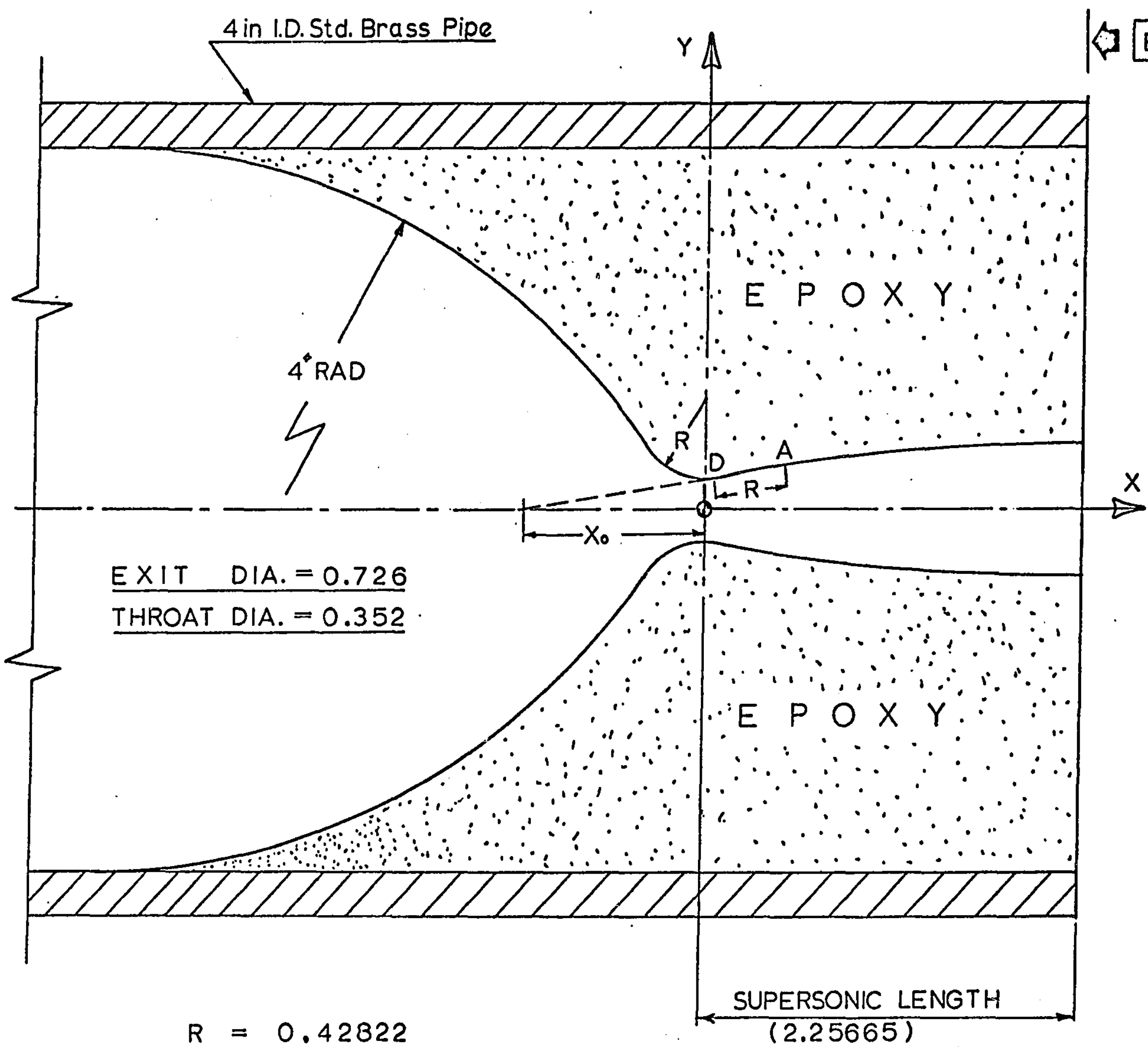

Coordinates of Nozzle

X	Y	Mach No.
2.25665	0.36300	3.00000
1.93954	0.35399	2.90000
1.65873	0.34399	2.80000
1.40846	0.33267	2.70000
1.18433	0.31979	2.60000
0.98294	0.30516	2.50000
0.80166	0.28861	2.40000
0.63842	0.26998	2.30000
0.49158	0.24912	2.20000
0.49084	0.24900	2.19893

All Measurements are in INCHES

⊕ Indicates WORK-POINT

$R = 0.42822$

$X_o = 1.07667$

$X_D = 0.06718$

$Y_D = 0.18170$

FIG. 4 – DETAILS OF SUPERSONIC NOZZLE

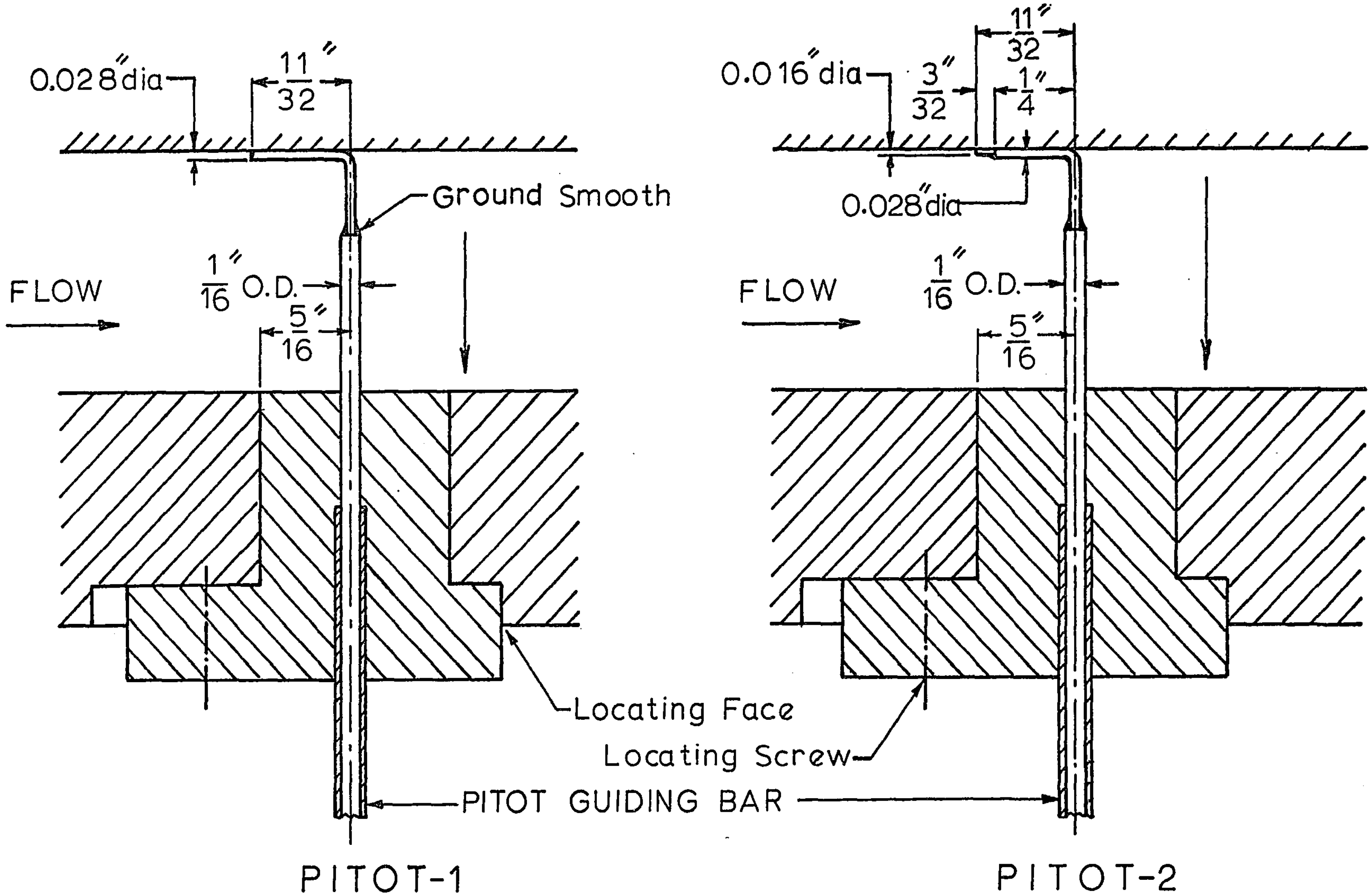

FIG. 5 - PITOT TUBES USED FOR THE MEASUREMENT OF SHEAR FLOW ACROSS THE PIPE.

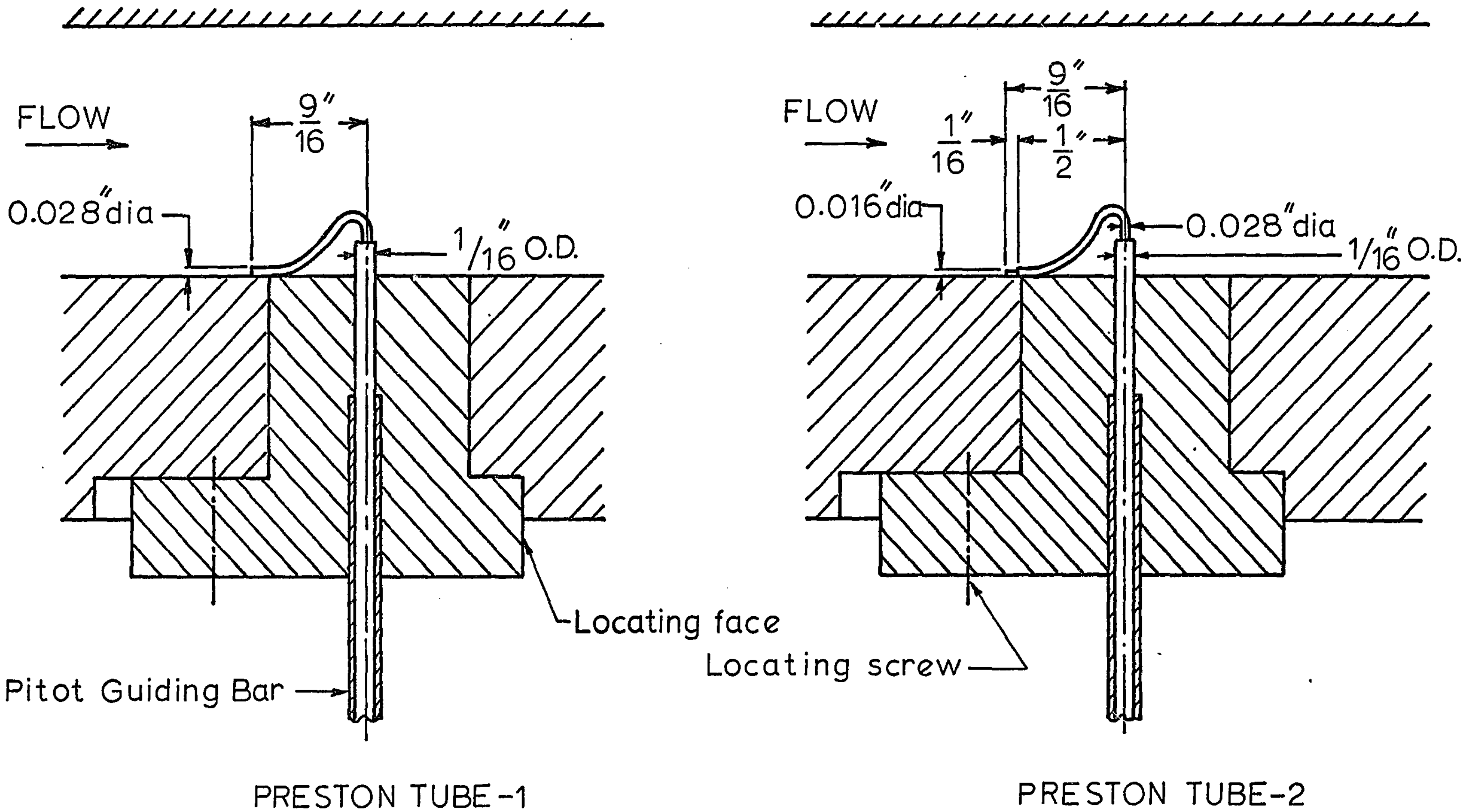

FIG. 6 — PITOT TUBES USED AS PRESTON TUBES FOR THE MEASUREMENT OF SKIN-FRICTION.

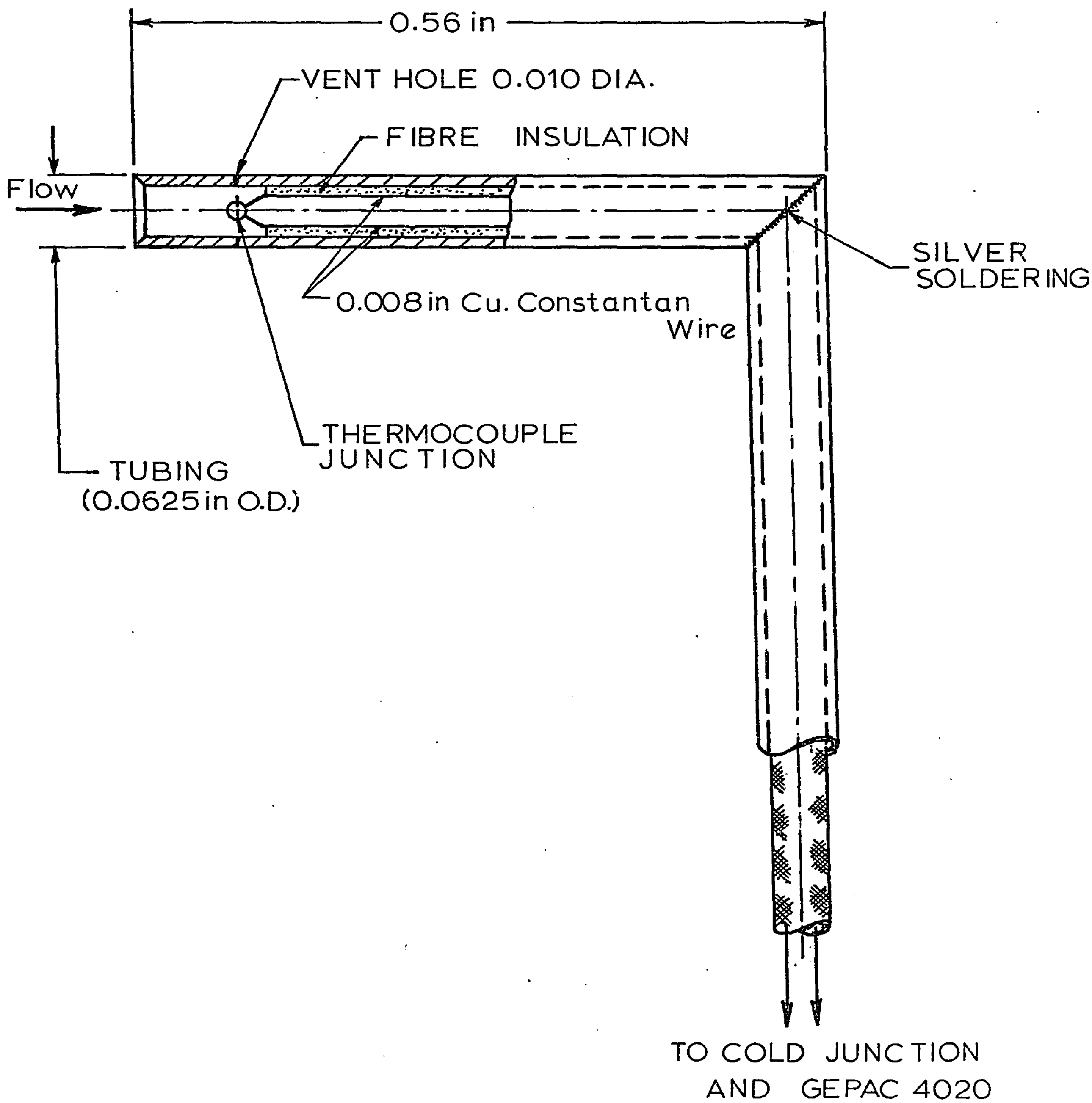

FIG. 7 – PROBE FOR MEASURING TOTAL TEMPERATURE OF FLOW ACROSS THE PIPE.

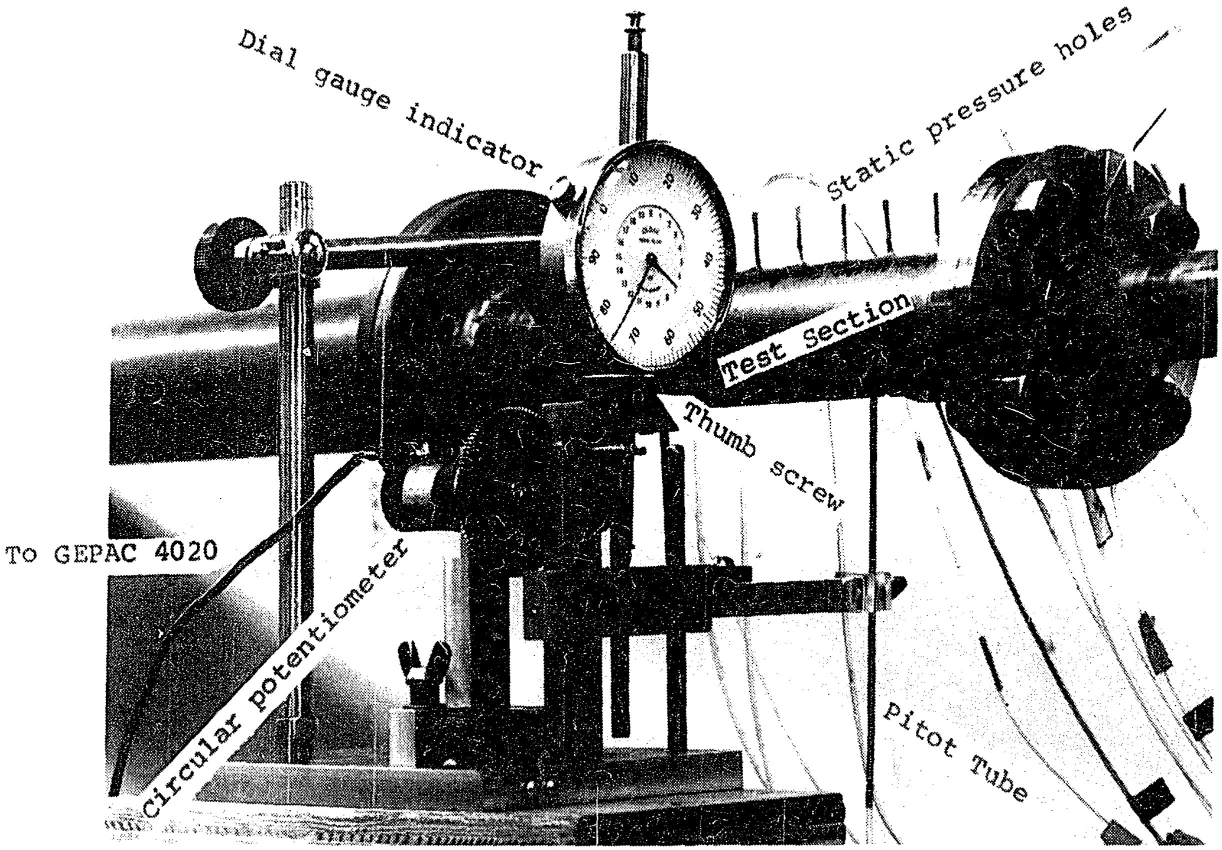

Fig. 8 - Photograph showing the Arrangement for Traversing the Pitot Tube and the Temperature Probe.

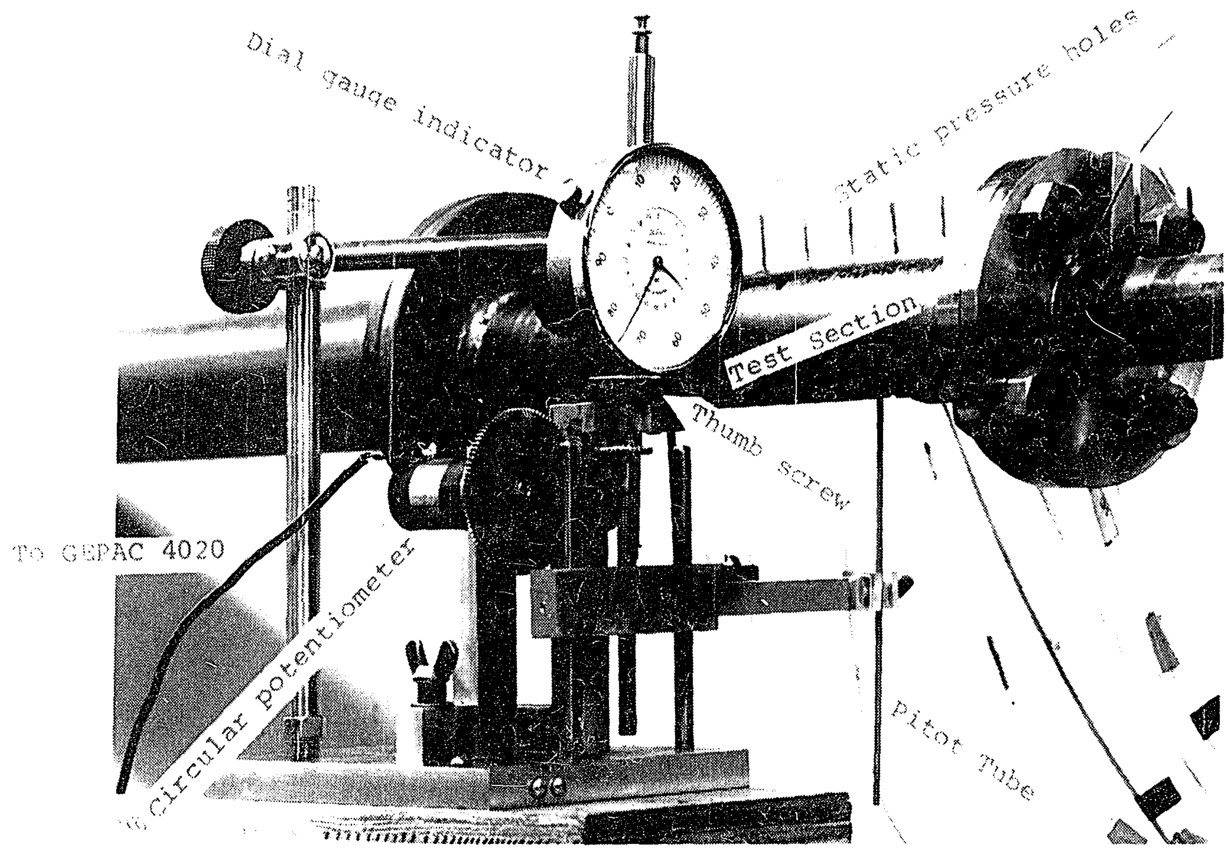
Dial gauge indicator
Static pressure holes
Test Section
Thumb screw
To GEPAC 4020
Circular potentiometer
Pitot Tube

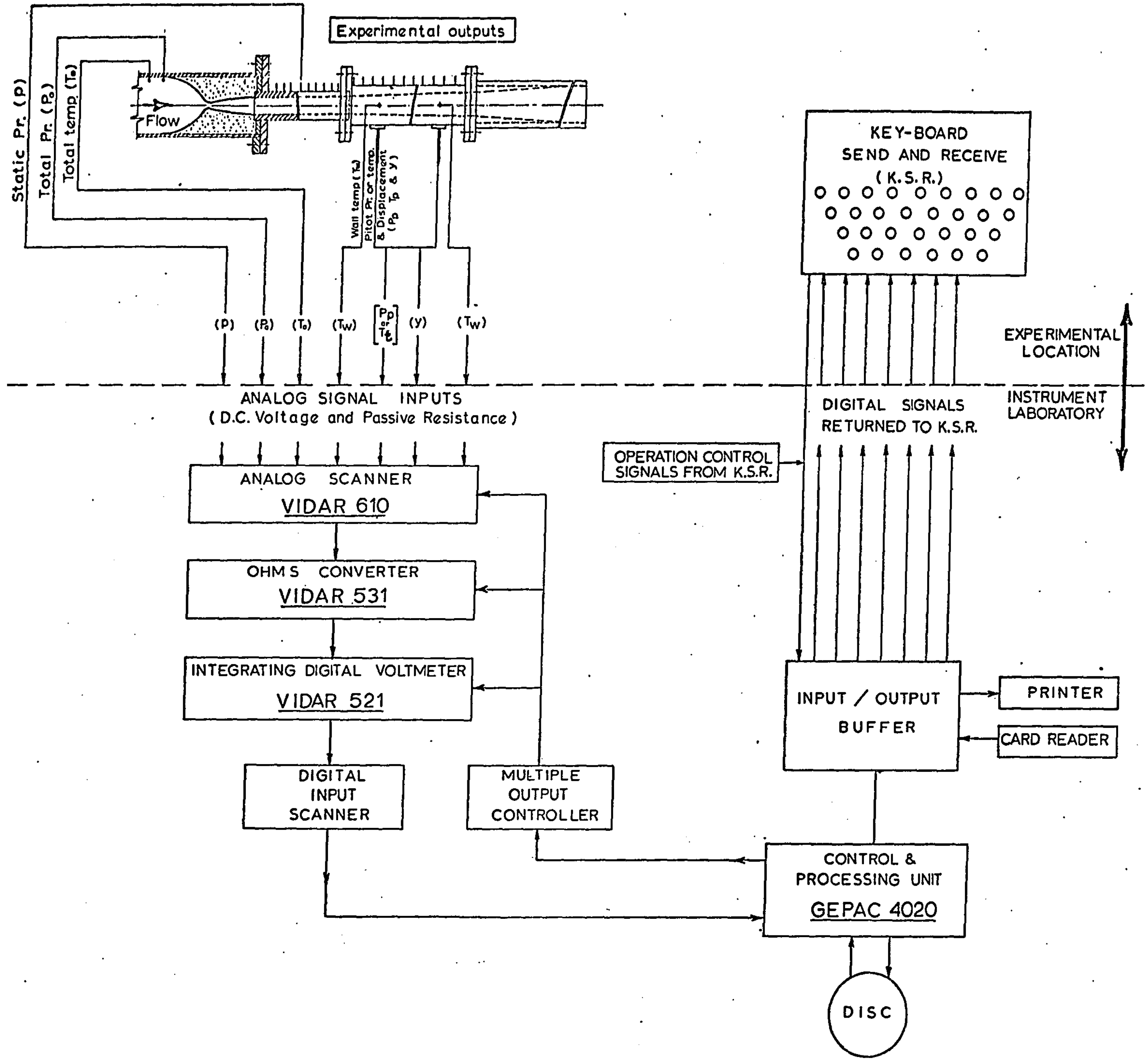

FIG.9 – SCHEMATIC OF THE INSTANTANEOUS DATA ACQUISTION ARRANGEMENT

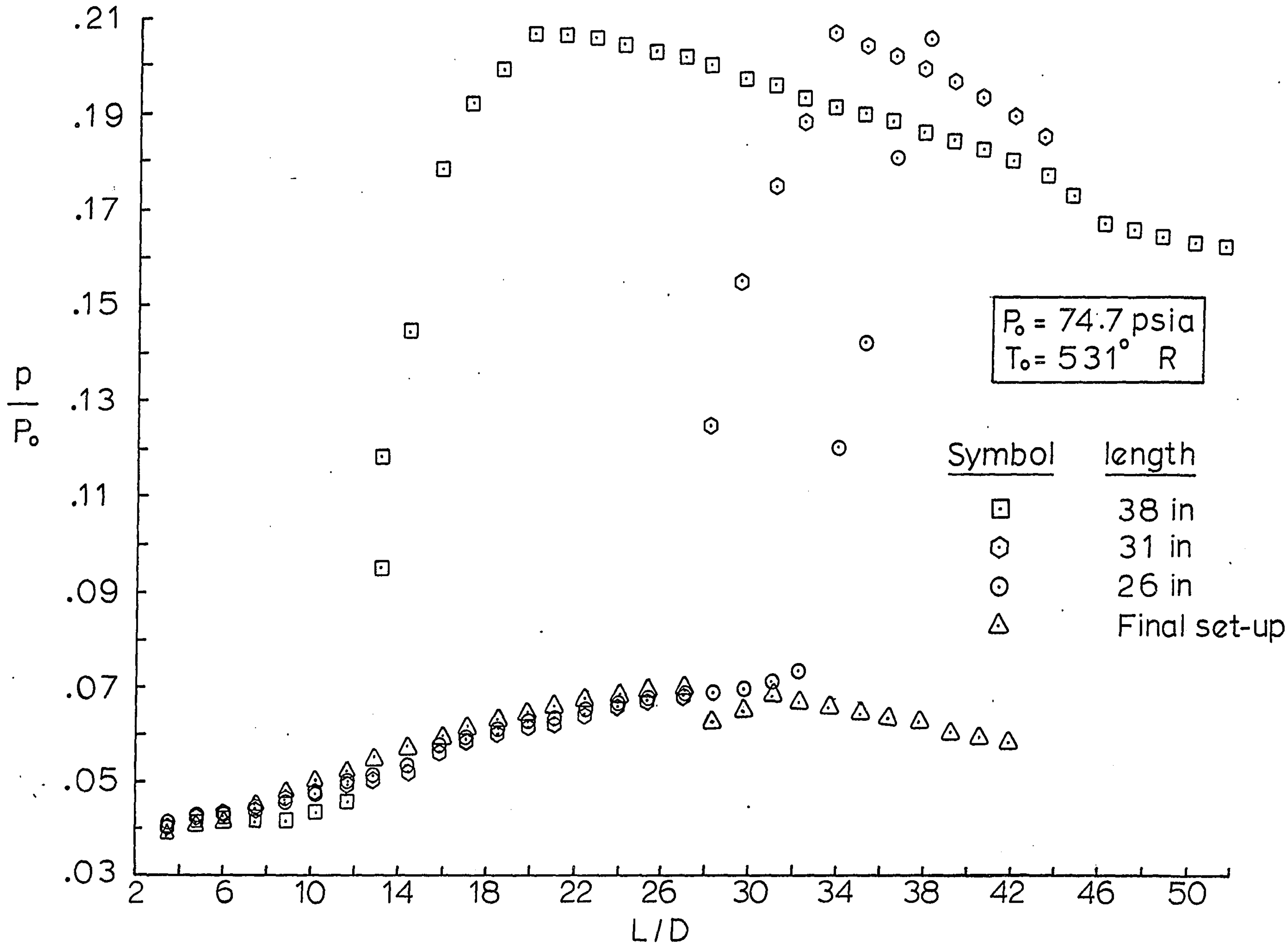

FIG.10 — PRESSURE DISTRIBUTION ALONG THE PIPE OF DIFFERENT LENGTHS.

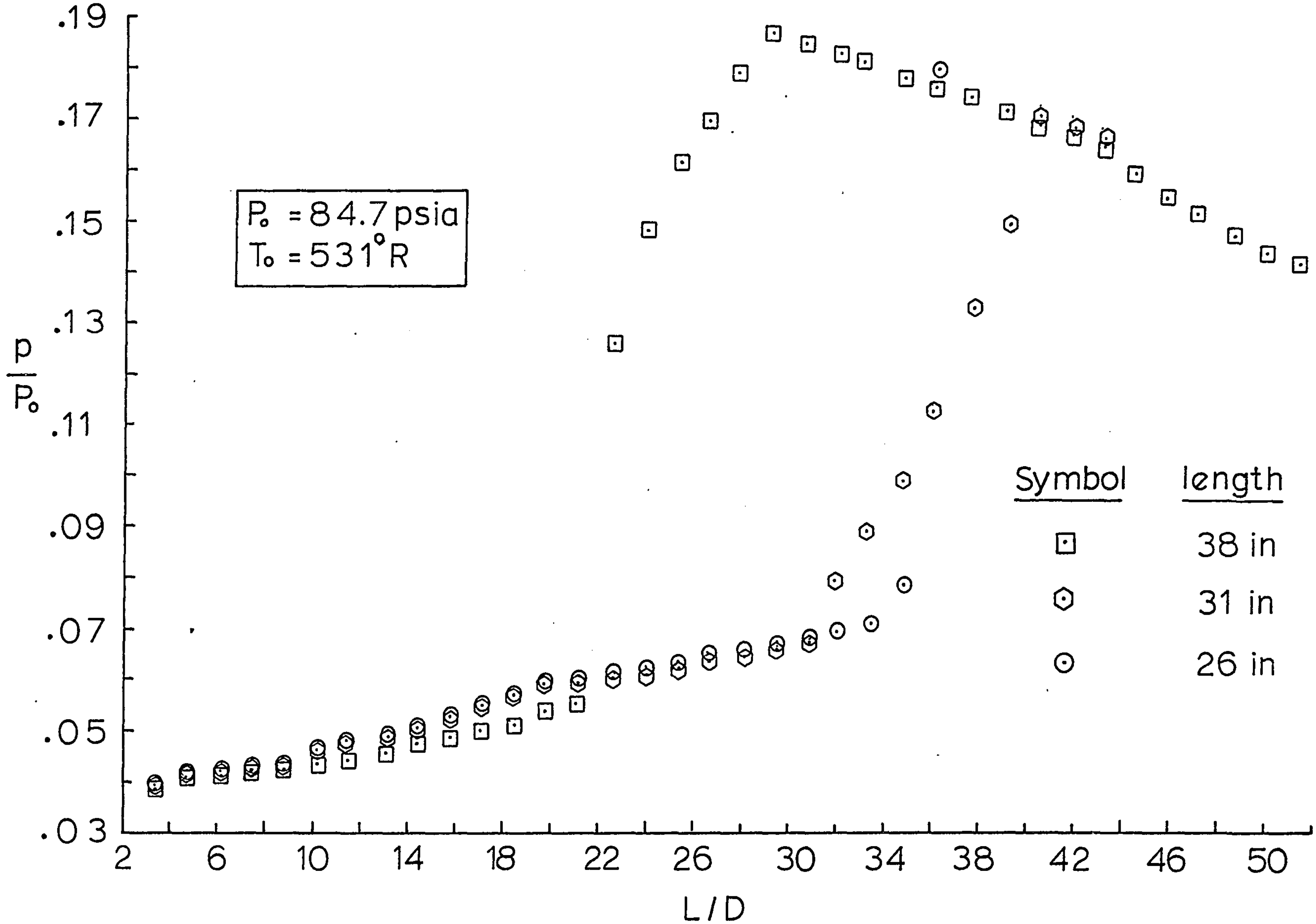

FIG.11 – PRESSURE DISTRIBUTION ALONG THE PIPE OF DIFFERENT LENGTHS.

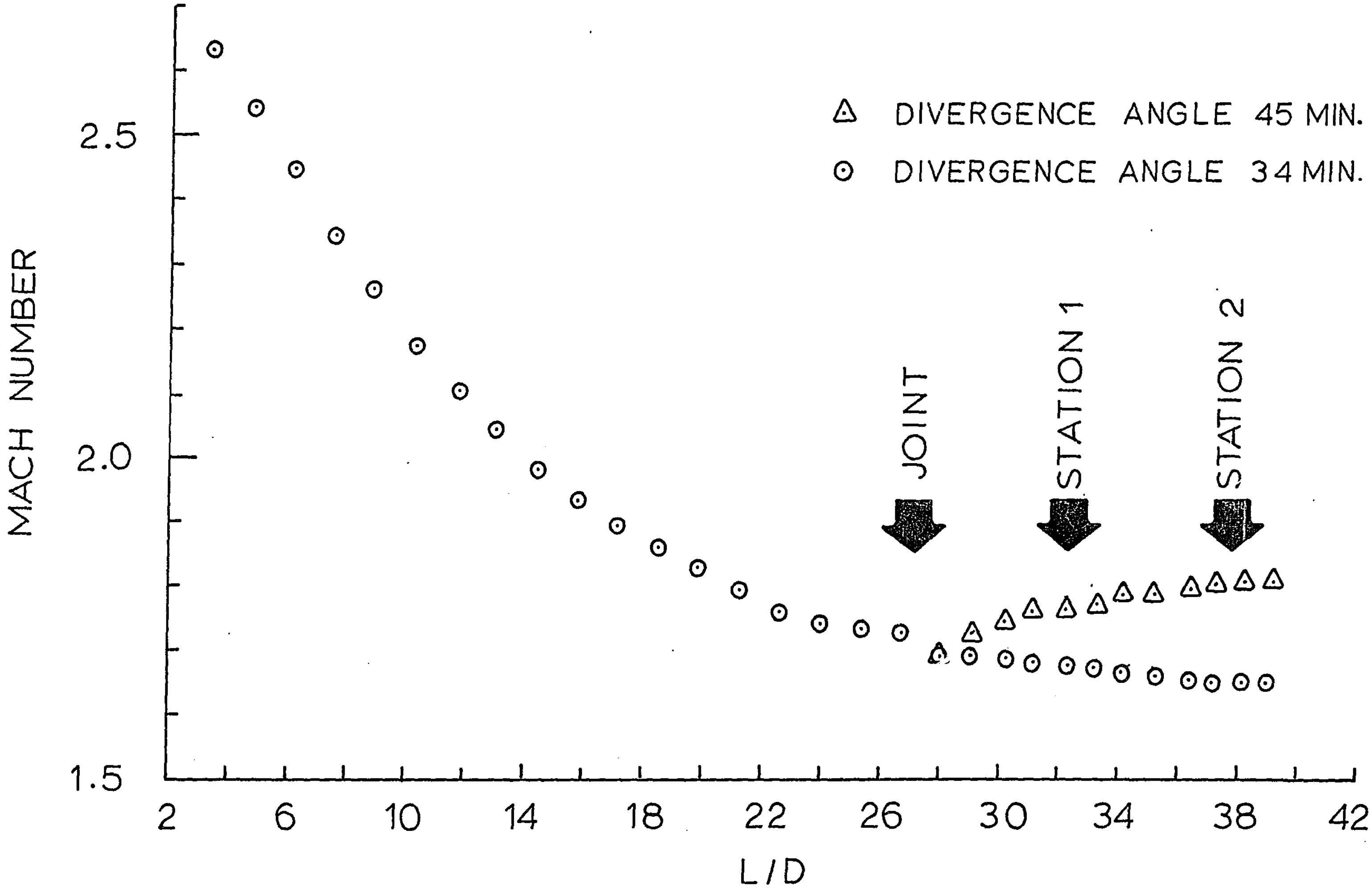

FIG.12 – MACH NUMBER DISTRIBUTION ALONG THE TEST SECTION
(FINAL SET-UP)

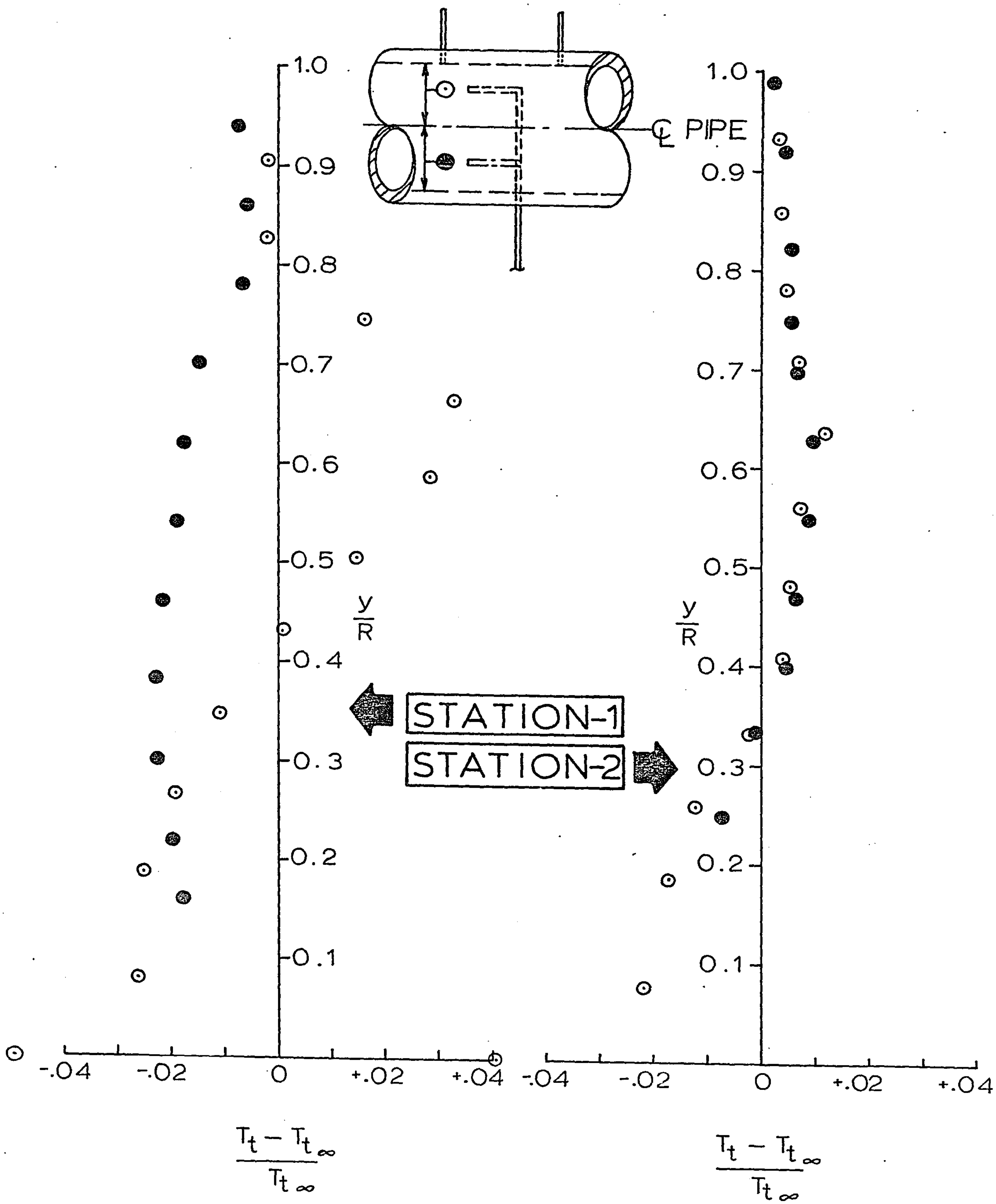

FIG.13 — TOTAL TEMPERATURE DISTRIBUTION ACROSS THE PIPE.

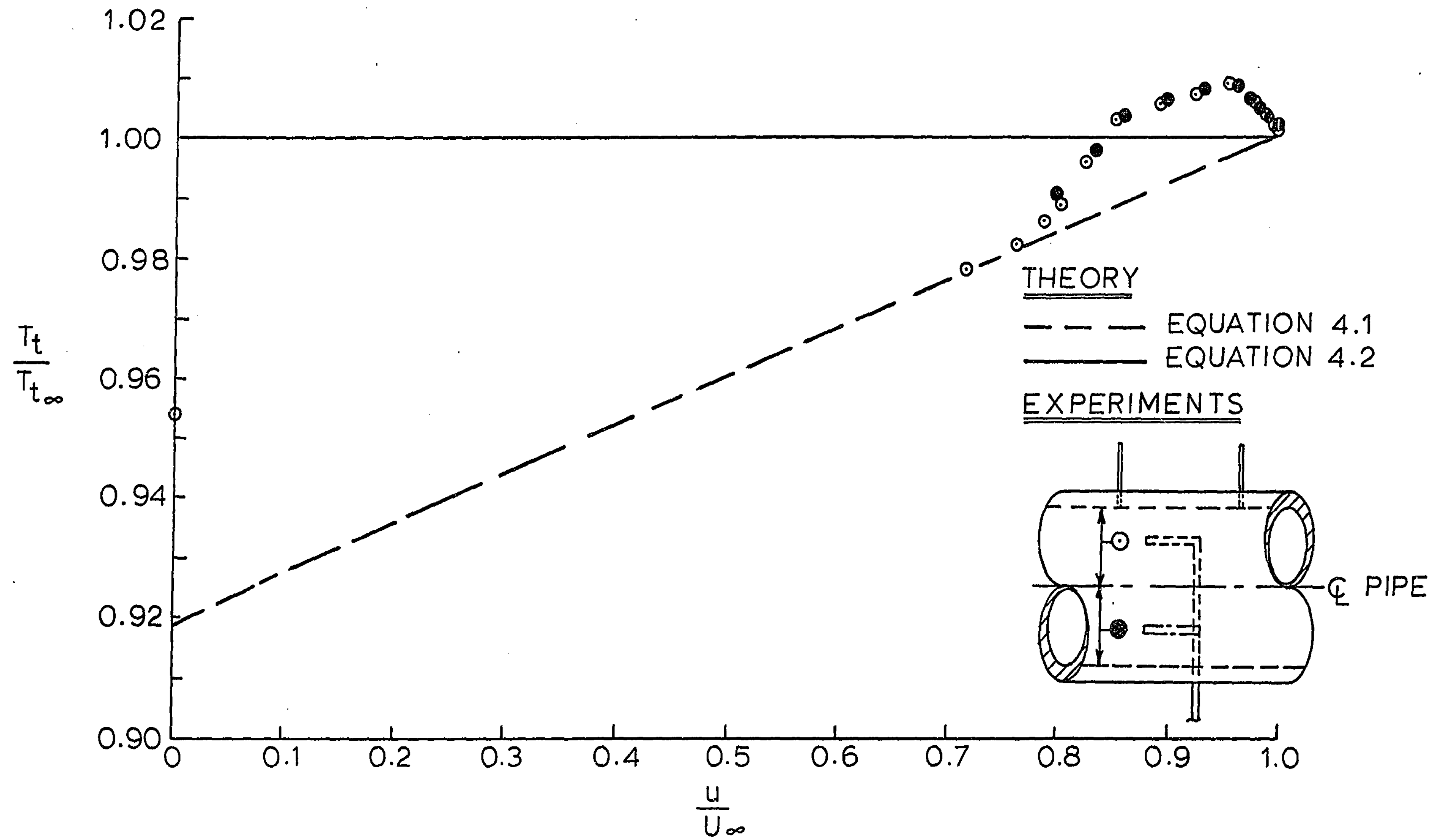

FIG. 14 TOTAL TEMPERATURE DISTRIBUTION ACROSS THE PIPE AT STATION 2.

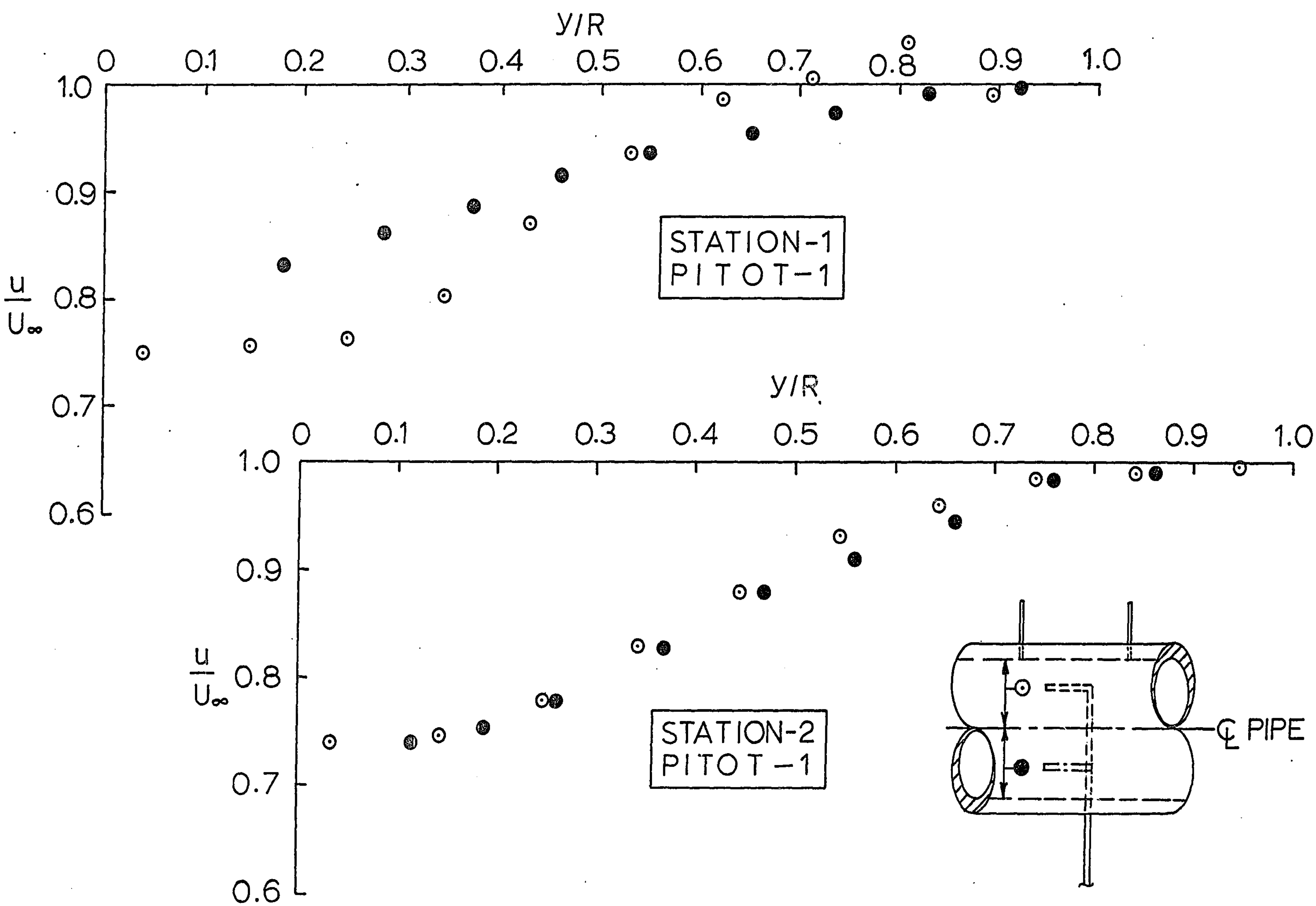

FIG.15 — VELOCITY DISTRIBUTION ACROSS THE PIPE

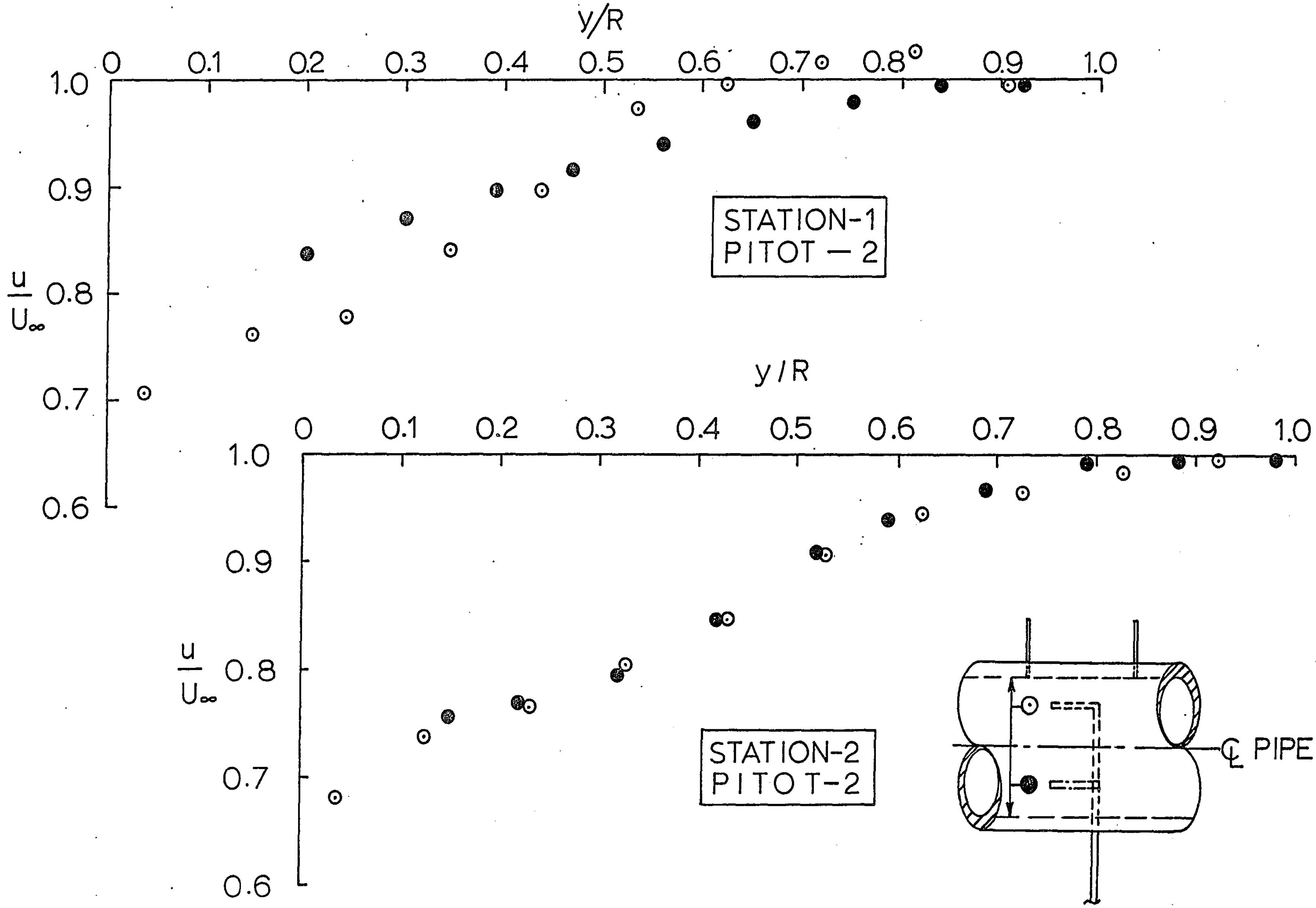

FIG.16 — VELOCITY DISTRIBUTION ACROSS THE PIPE

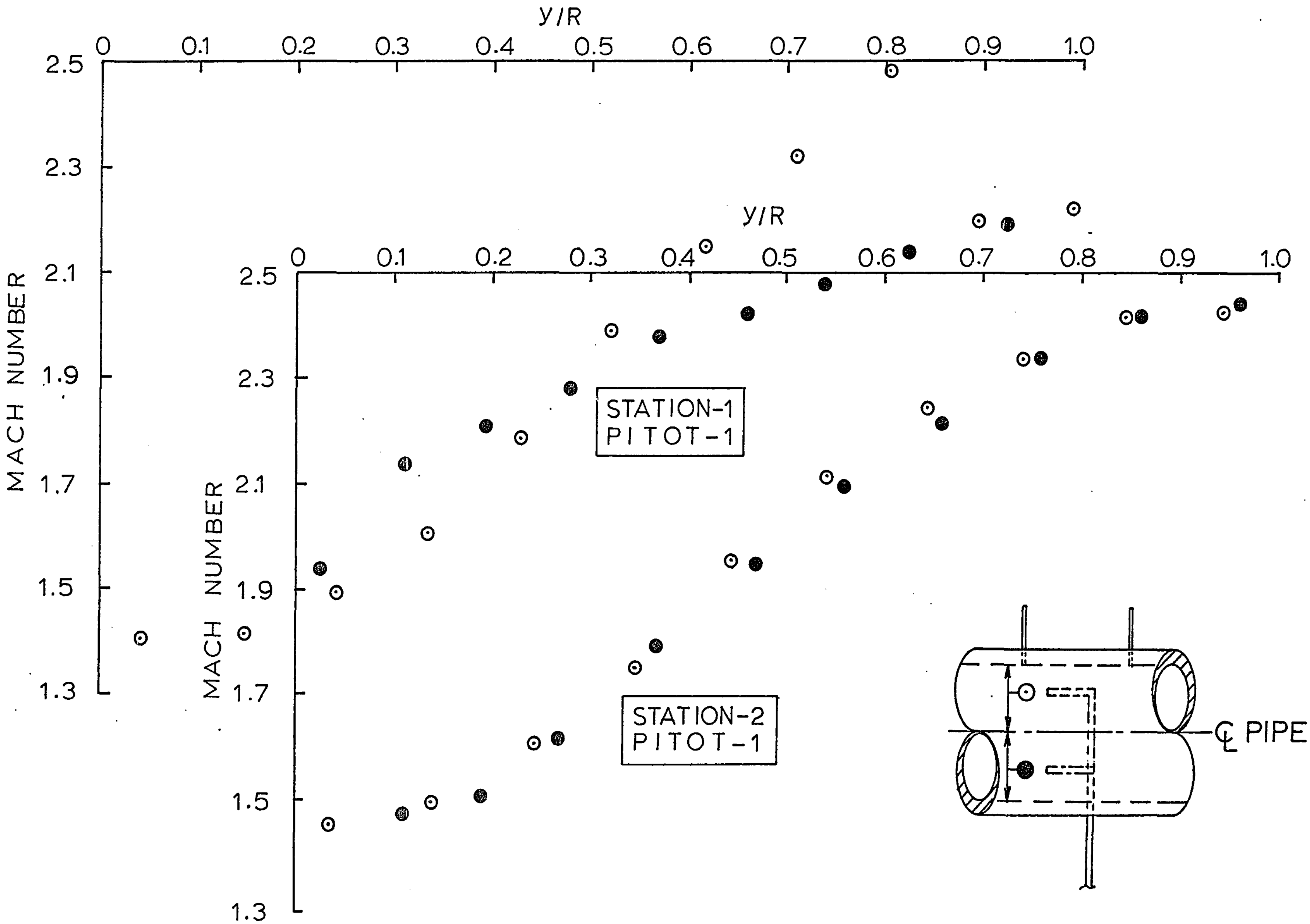

FIG.17— MACH NUMBER DISTRIBUTION ACROSS THE PIPE

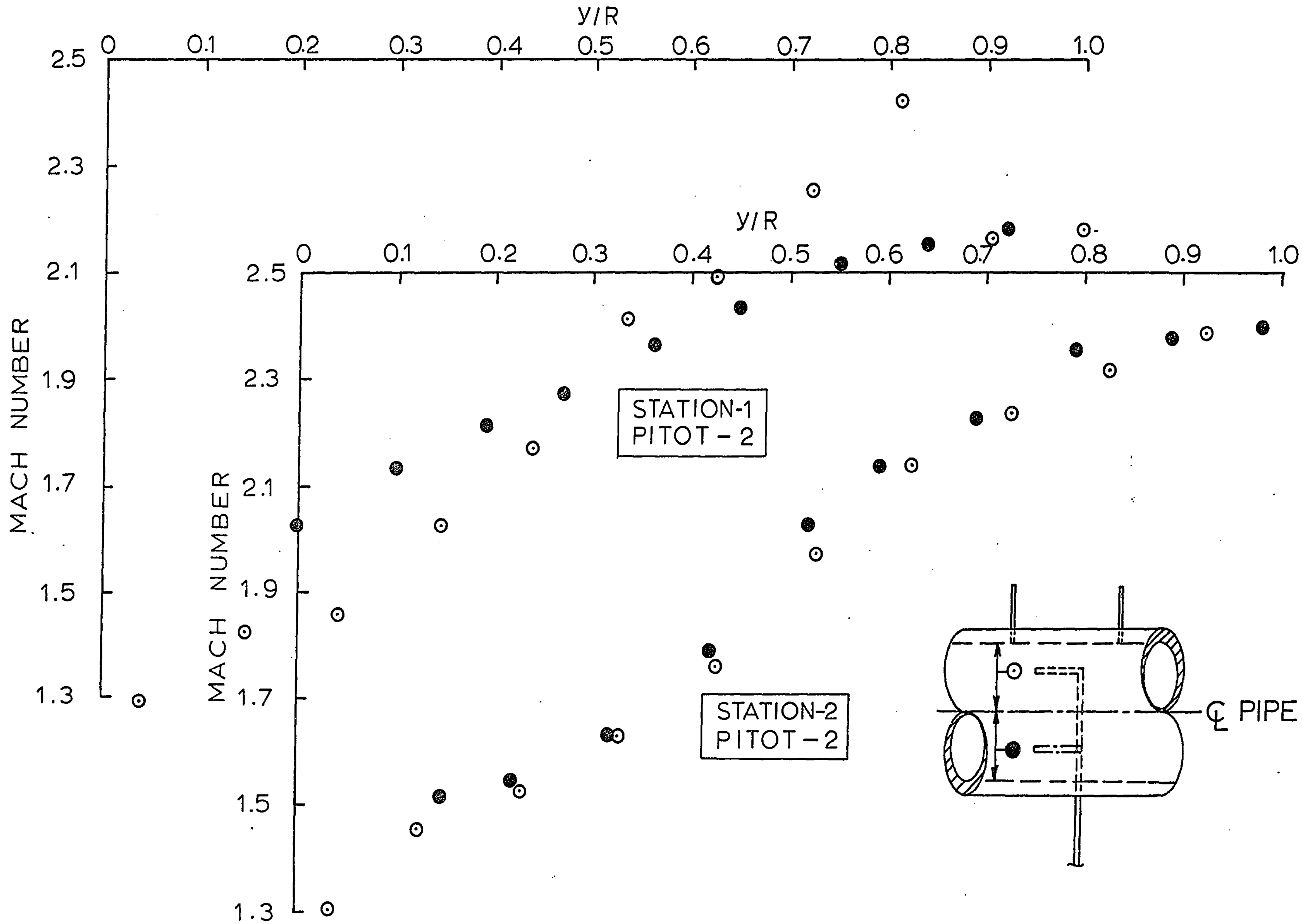

FIG.18—MACH NUMBER DISTRIBUTION ACROSS THE PIPE

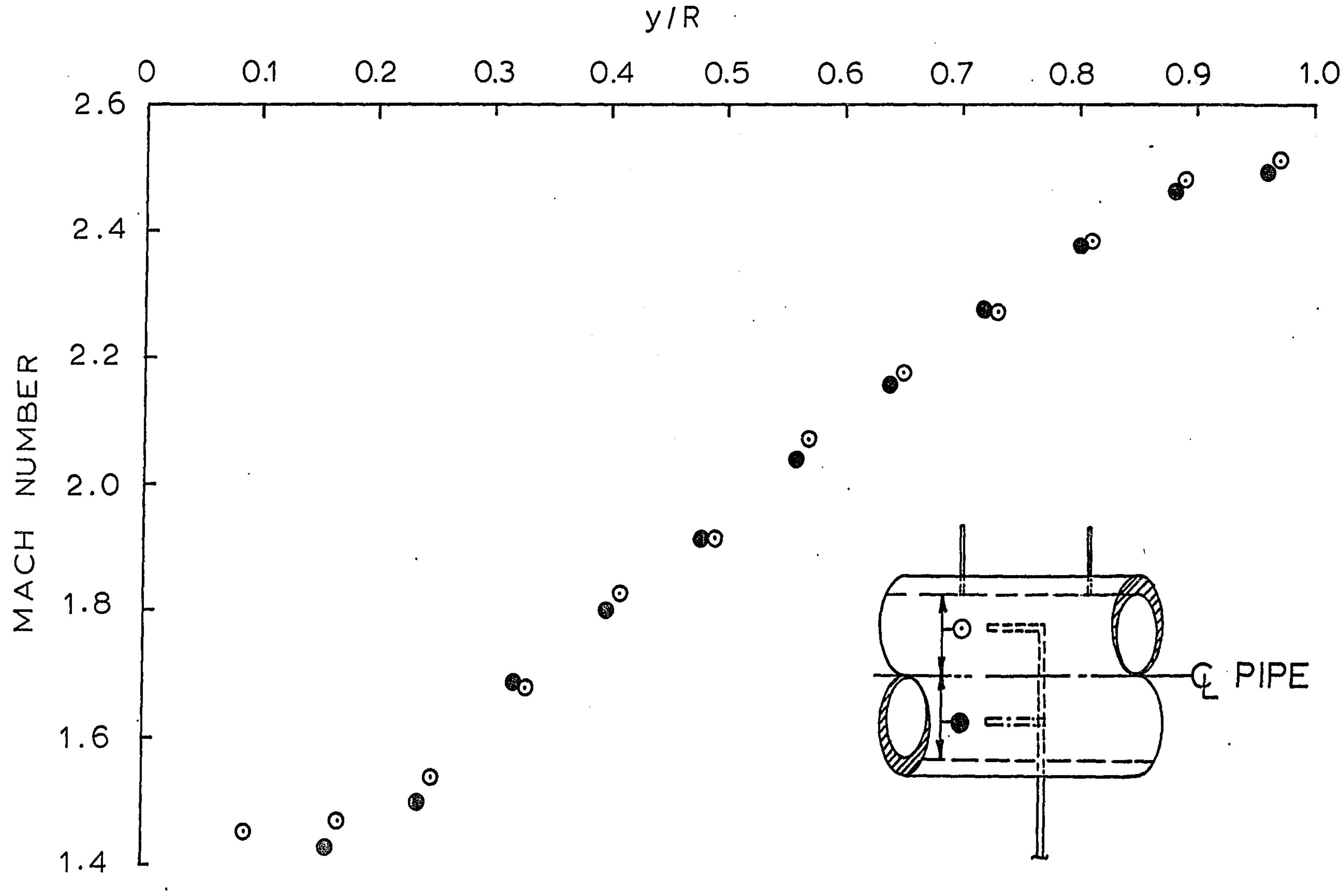

FIG.19 — MACH NUMBER DISTRIBUTION ACROSS THE PIPE AT L/D=25
(BEFORE ATTACHING THE DIVERGING TEST PIPE)

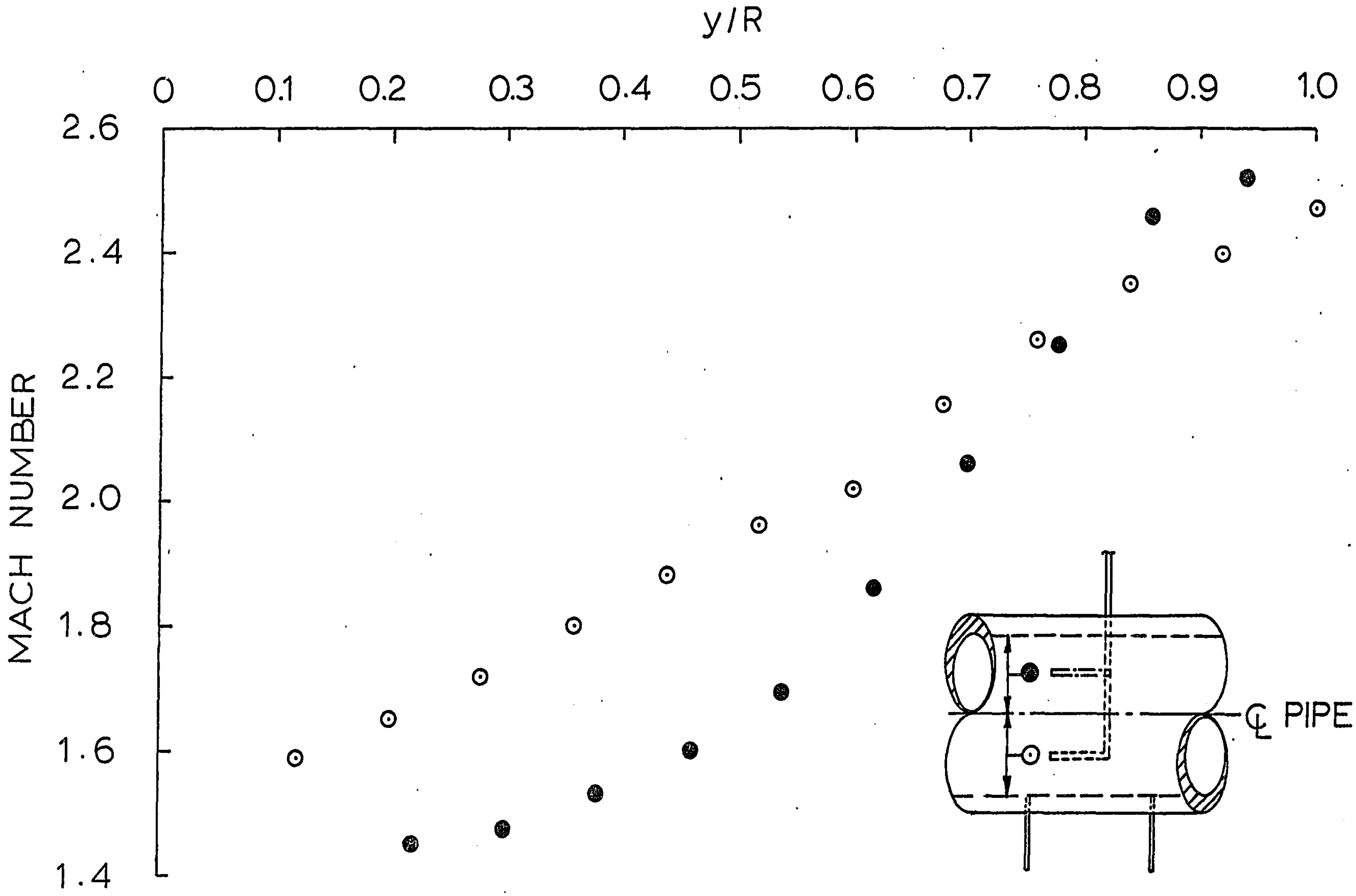

FIG. 20 – MACH NUMBER DISTRIBUTION ACROSS THE PIPE AT STATION 1 AFTER 180° ROTATION.

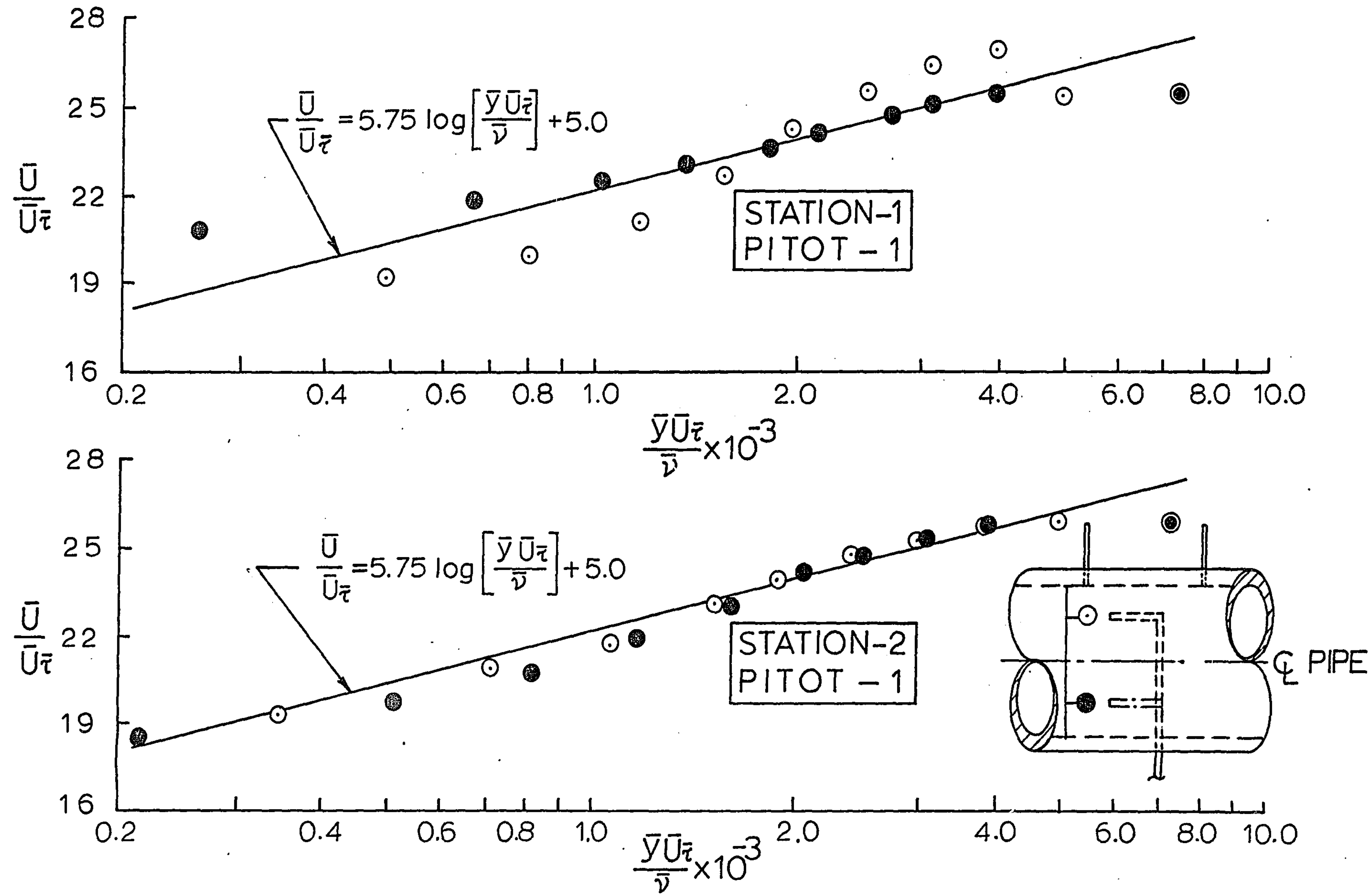

FIG. 21 VELOCITY PROFILES IN TRANSFORMED LAW OF THE WALL CO ORDINATES. (SKIN FRICTION FROM PRESTON TUBE)

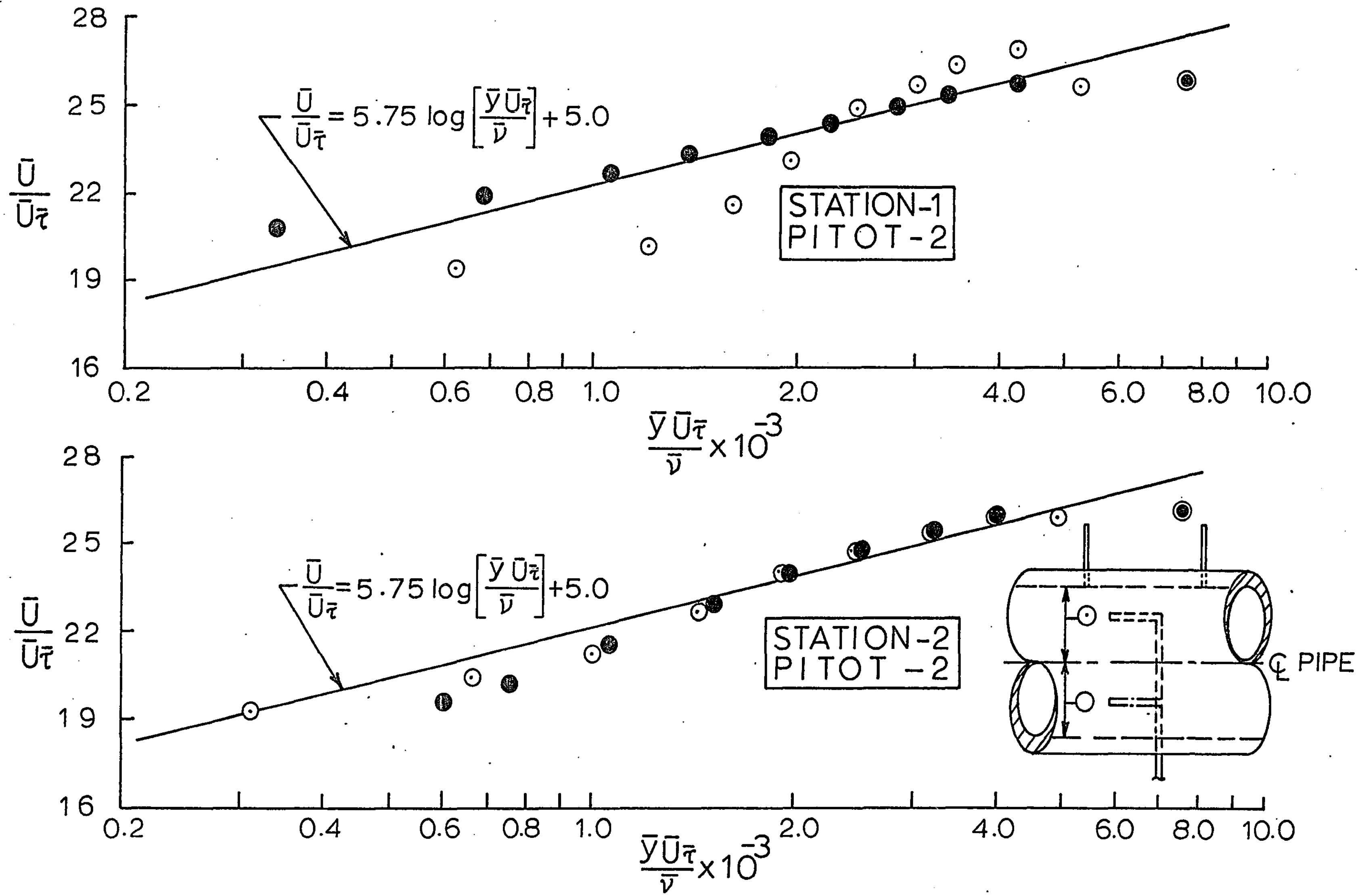

FIG. 22 - VELOCITY PROFILES IN TRANSFORMED LAW OF THE WALL CO-ORDINATES. (SKIN FRICTION FROM PRESTON TUBE)

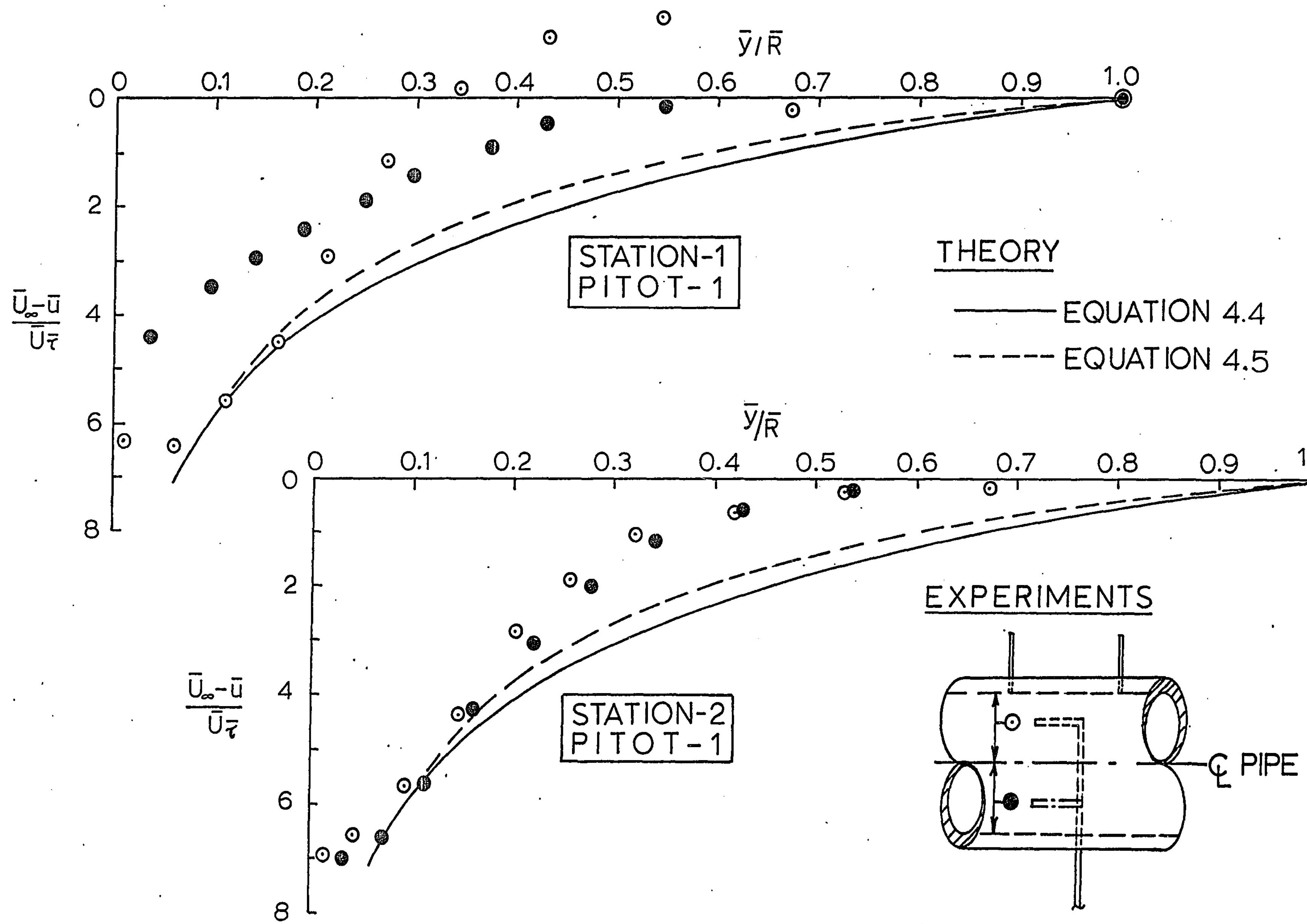

FIG. 23 – VELOCITY PROFILES IN TRANSFORMED DEFECT LAW CO-ORDINATES. (SKIN-FRICTION FROM PRESTON TUBE)

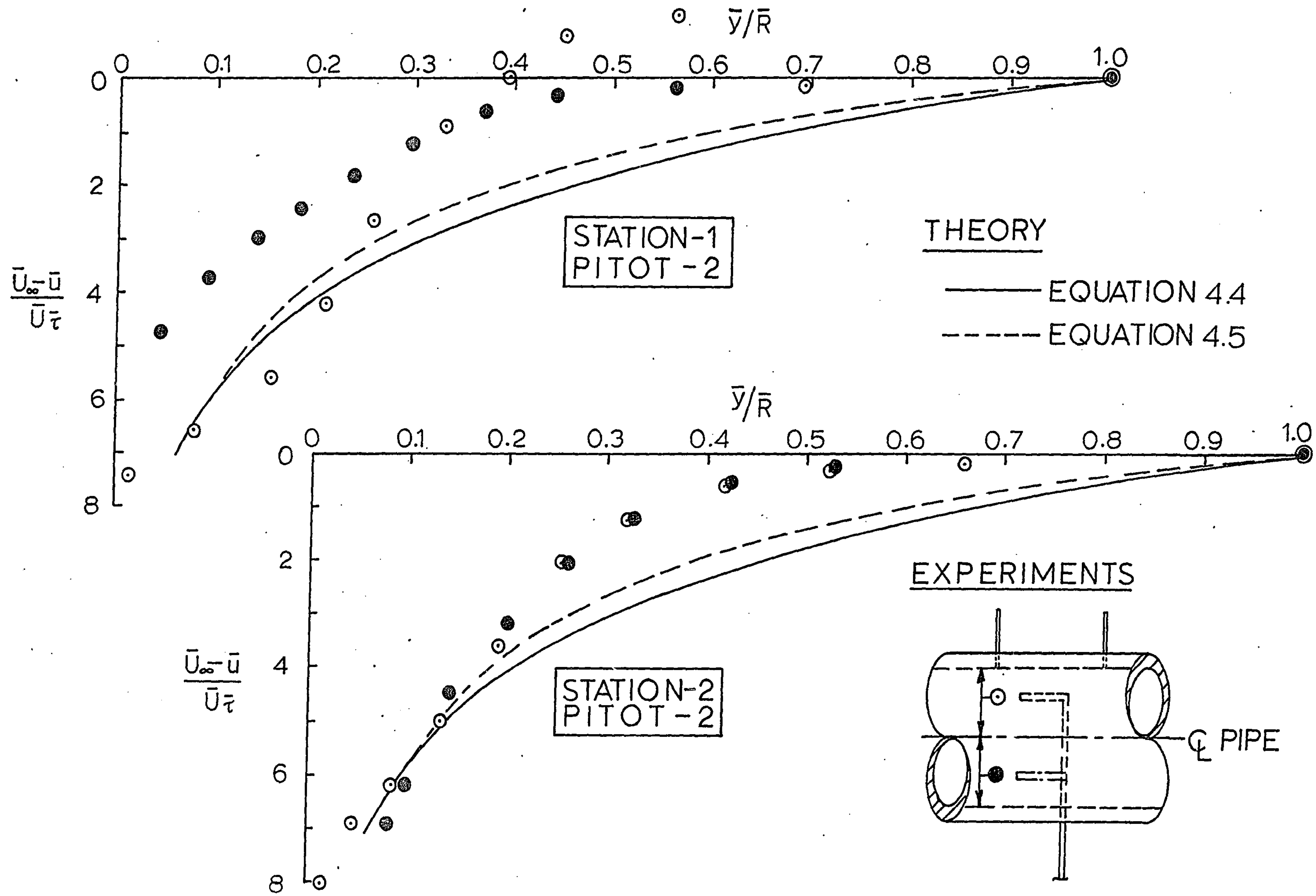

FIG. 24 - VELOCITY PROFILES IN TRANSFORMED DEFECT LAW CO-ORDINATES (SKIN-FRICTION FROM PRESTON TUBE)

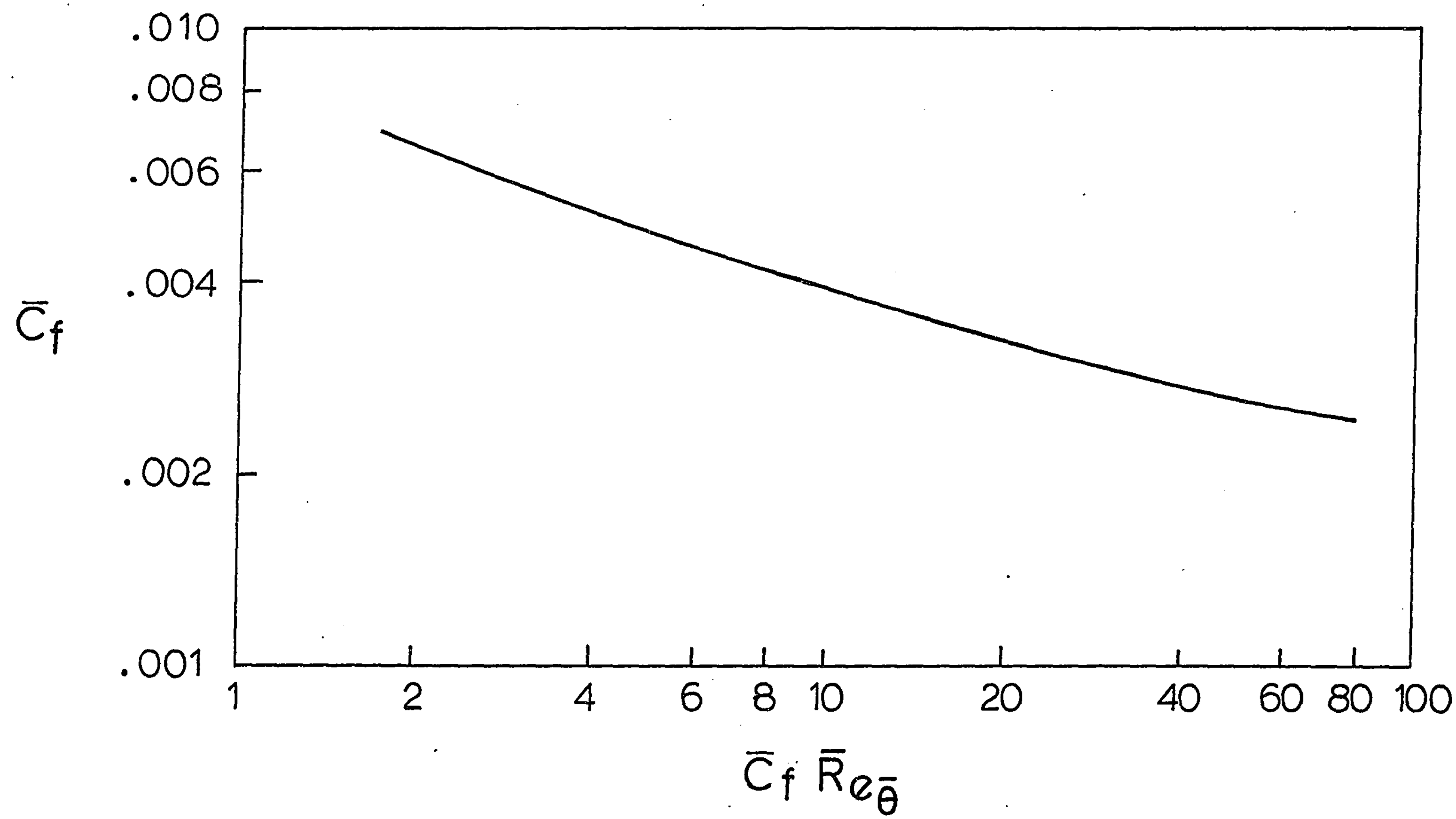

FIG. 25 — DEPENDENCE OF $\bar{C}_f$ ON $\bar{C}_f \, \bar{R}_{e_{\bar{\theta}}}$